Annual Review of Heat Transfer, Vol. 16 (2013)

CHAPTER 13

THERMAL TRANSPORT IN PHASE CHANGE MEMORY MATERIALS

Elah Bozorg-Grayeli,[1,*] *John P. Reifenberg,*[2] *Mehdi Asheghi,*[1] *H.-S. Philip Wong,*[3] & *Kenneth E. Goodson*[1]

[1] Department of Mechanical Engineering, Stanford University, Stanford, CA 94305, USA

[2] Alphabet Energy, San Francisco, CA 94103, USA

[3] Department of Electrical Engineering, Stanford University, Stanford, CA 94305, USA

*Address all correspondence to Elah Bozorg-Grayeli E-mail: ebozorgg@stanford.edu

Phase change memory uses brief pulses of electrical current to induce phase transitions in chalcogenide material regions with dimensions near or even far below 50 nm. The strongly differing electrical conductivities of the crystalline and amorphous phases allow data storage at densities in excess of terabits per square inch. Nanoscale conduction heat transfer governs the figures of merit in these devices, which include the energy and time required for switching, and has received much attention through both measurements and simulations over the last two decades. This chapter reviews the recent progress on thermal conduction phenomena relevant for phase change memory, including a summary of the physical mechanisms involved as well as the most useful simulation and measurement techniques. Experimental work has focused on separating the intrinsic and boundary resistances of thin film phase change materials, as well as the individual contributions of electrons and phonons to the effective conductivity of the hexagonal crystalline phase. Simulations have focused on improving device geometries and switching characteristics, and continue to need improvements in the areas of crystallization modeling and the impact of phase distribution on electrical and thermal transport. Future research requires a more detailed understanding of electron-phonon coupling and its impact on electrical and thermal conduction in the crystalline phase, as well as greater insight into thermoelectric transport and its impact on device behavior. This progress will be critical for the development of innovative memory strategies including multibit storage.

1. INTRODUCTION

Interest in the fundamental study of chalcogenide phase change materials has accelerated over the past decade due to their application in high-density optical recording,[1,2] phase change memory (PCM) devices,[3,4] and, more recently, in thermoelectric power generation and cooling (TPG&C) technology.[5−7] First-generation PCM devices are beginning to enter the marketplace in multichip packages and handsets,[8] and show great potential for scalability.[9] Figure 1 shows that the number of papers studying chalcogenides for data storage has doubled every six or seven years during this time period. PCM devices rely on complex interactions between temperature, electrical fields and current transport, crystallization, and species diffusion processes.[10] The complexity of high-density phase change

ISSN: 1049–0787; ISBN: 978–1–56700–222–6/13/$35.00 + $00.00

© 2013 by Begell House, Inc.

NOMENCLATURE

A	area (m^2)
b	heater half-width (m)
C	volumetric heat capacity (J m^{-3} K^{-1})
C_{dim}	dimensionless parameter
c	sound speed (m s^{-1})
d	thickness (nm)
f	frequency (10^6 Hz)
G	electron-phonon energy transfer rate (W m^{-3} K)
K_{b}	Boltzmann's constant (J K^{-1})
k	thermal conductivity (W m^{-1} K^{-1})
L	heater length (m)
L_{WFL}	Lorenz coefficient (W Ω K^{-2})
n	number density (m^{-3})
Q	heating power (W)
q''	heat flux (W m^{-2})
R	thermal resistance (m^2 K W^{-1})
S_{dim}	dimensionless parameter
S	Seebeck coefficient (mV K^{-1})
T	temperature (K or °C)
v	velocity (m s^{-1})
Z_{apparent}	thermal transfer function
Z	electrical energy flux (W m^{-2} K^{-1})
ZT	dimensionless figure of merit

Greek Symbols

α	transmission coefficient
β_F	dimensionless parameter
γ	Sommerfeld parameter (J m^{-3} K^{-2})
θ	Debye temperature
λ	mean free path (m)
ρ	electrical boundary resistance (Ω m^2)
σ	electrical conductivity (Ω^{-1} m^{-1})
τ	characteristic time scale (s)

Subscripts

b	boundary
D	Debye
DMM	diffuse mismatch model
e	electron
e-p	electron-phonon
f	Fermi
l	longitudinal
p	phonon
s	substrate
t	transverse
x	in-plane
y	cross-plane

(PC) optical recording technology is comparable to that of PCM due to challenges associated with subdiffraction optical writing and read-back. PC materials in high-density data storage applications undergo millions of temperature cycles of unprecedented magnitude, $\Delta T \sim 600°\text{C}$, where temporal and spatial temperature gradients of $\sim 10^9$°C/s and $\sim 10^3$°C/nm prevail. The importance of PC thermal properties in the operation, reliability, and scaling of high-density data storage devices explains the growing interest in their study.

Although recent progress has been rapid, the physical principles behind PCM and the first devices using these principles are over 40 years old.[11–14] In PCM devices, a chalcogenide thin film switches reversibly between the bistable polycrystalline (SET, low resistivity) and amorphous (RESET, high resistivity) states, shown in Fig. 2(a), and, schematically, in Fig. 2(b).[15] In the phase change material $Ge_2Sb_2Te_5$, the crystalline states are

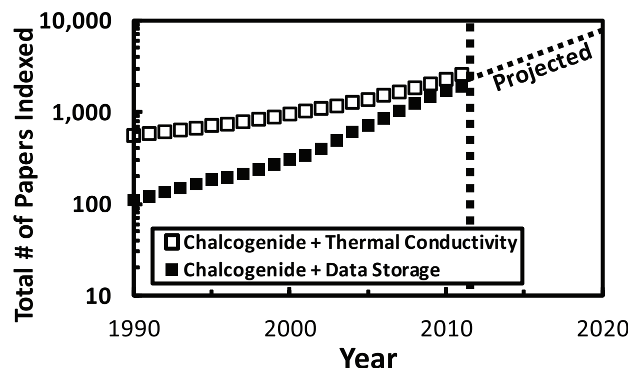

FIG. 1: Interest in chalcogenides for data storage and their thermal properties, measured by number of papers indexed by Google (scholar.google.com accessed 11/01/2011), has grown almost exponentially over the past 15 years.

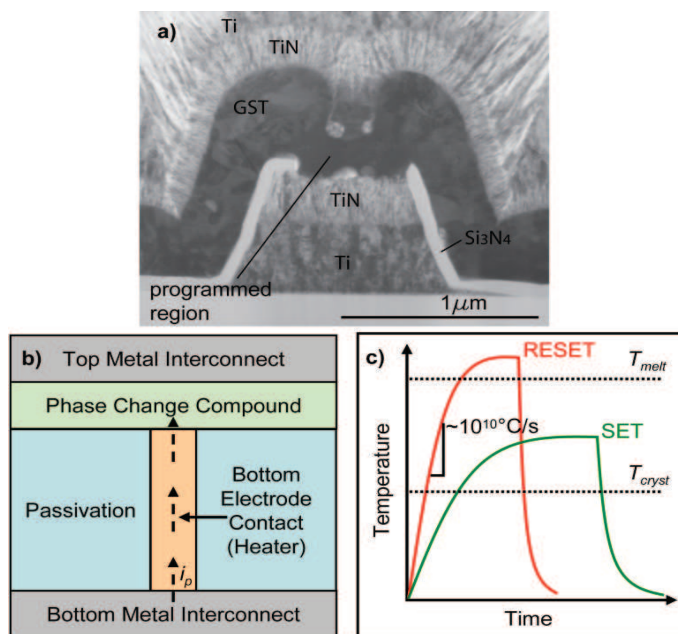

FIG. 2: (a) Transmission electron microscopy (TEM) image of a PCM cell that has been subjected to a RESET process.[15] (b) Schematic of a simple PCM cell with programming current i_{p}. (c) Schematic of the temperature history during programming events. $T_{\mathrm{crys}} \approx$ 300°C and $T_{\mathrm{melt}} > 600$°C. The switching time is highly dependent on the thermal decay time of the cell, but can be as low as tens of nanoseconds.

face-centered cubic (FCC) and hexagonal close-packed (HCP). The FCC state is similar to the rock salt structure, with small deviations due to the varying radii of the atoms involved. As a result, the Ge-Te and Sb-Te bonds are slightly larger than expected for an ideal FCC structure.[16] Joule heating, caused by a controlled current pulse, induces structural changes

between these phases. Rapid melting ($T > 600°C$) and quenching of the crystalline phase change material at $\sim 10^{10}$°C/s freezes it into the glasslike amorphous phase. Sustained heating above the glass temperature, ~300°C, causes the amorphous phase to transition back to the crystalline phase. Figure 2(c) schematically depicts the temperature history during programming. Threshold switching, the process whereby an amorphous semiconductor switches into a low-resistivity state in the presence of a large electric field,[11] permits the amorphous-to-crystalline transition to occur at similar voltages as the crystalline to amorphous transition. The heating and quenching process can occur up to 10^{10}–10^{12} times.[17]

A functional phase change memory array of 128 Mb (90 nm node) has been demonstrated.[18] Favorable scaling is often cited[3,4,17] as one of the key advantages of PCM over other nonvolatile memory (NVM) technologies, and it is suggested that PCM may be scalable well beyond the 50 nm node.[4,19] There have been numerous efforts to discover novel cost-effective methods for fabrication in the sub-50 nm regime to overcome the difficulties associated with electron beam lithography. Several groups[20−22] demonstrated functioning devices using $Ge_2Sb_2Te_5$ (GST) nanowires (d = 30–500 nm). However, challenges associated with proper alignment and integration processes remain. Other groups have developed bottom-up self-assembly–based fabrication processes[23] that produce highly ordered PC nanoparticles of dimensions ~10–20 nm. This process can be also utilized for growth of highly ordered Ge nanowires (NWs) as the bottom electrical contact for PCM, further reducing the contact area and programming current.[24]

The widespread adoption of PC materials in high-density optical phase change recording (e.g., CD-RW, DVD-RW) predates many of the recent advances in PCM. In high-density optical recording, a tightly focused laser heats a small spot in a PC layer sandwiched between dielectric thin films. Laser absorption in the PC layer causes phase transitions between the crystalline and amorphous phases, which have a strong contrast in optical reflectivity. Data are read by measuring the reflected intensity of a low-power read laser. The main challenge facing PC optical recording is the diffraction limit. The super-resolution near-field structure (super-RENS) has emerged to overcome this limitation by introducing a layer of randomly dispersed Ag or SbTe nanoparticles.[1] Recently, Small et al.[1] demonstrated that areal-density and readback signal noise characteristics can be considerably improved in a nanopatterned PC medium, but offered no commercially viable manufacturing process to realize the technology. Self-assembled PC nanoparticles are a promising candidate for integrating the super-RENS and patterned PC media schemes into a single media stack.

More recently, Castro et al.[25] reported the first evidence of the thermoelectric effect and its dramatic impact on the characteristics of linear PCM devices. Chalcogenide PC materials have also attracted much attention as candidates for thermoelectric power conversion applications.[5,7] The figure of merit for power generation, known as the power factor, is $\sim 10^{-3}$ W m^{-1} K^{-2} for high-performance thermoelectric materials compared to the reported values of 4×10^{-4} and 5×10^{-3} W m^{-1} K^{-2} for bulk,[5] and superlattice $(Bi_{0.2}Sb_{0.8})_2Te_3$-Sb_2Te_3[7] PC materials, respectively. Power factors comparable to or larger than those of high-performance thermoelectric materials[26] may be within reach using fine-grain PC thin film and nanoparticles due to enhancement in the phonon drag component of the

Seebeck coefficient.[27,28] Further enhancements will be possible due to the reduced thermal conductivity of the thin film PC materials compared to those of the bulk samples.[29,30] Table 1 provides a baseline summary of the existing data on thermal, electric, and thermoelectric properties of GST.

Thermal design and engineering play an important role in optimizing the performance of both optical and PCM devices. In optical storage media, mark-edge jitter dominates the read signal noise. Jitter, storage density, and speed are all influenced by the thermal properties of the constituent films.[1,31] In PCM, thermal properties influence virtually every figure of merit including the programming current, scalability, reliability, and cross talk, among others.[4,32–34] While compact models demonstrate the role of the total device thermal resistance,[4,32,33,35,36] detailed finite element models discern the importance of the spatial distribution of thermal properties.[32,34,37] Device studies confirm that increasing interfacial[38–40] and volumetric[15,41] thermal resistances, and confining heat generation[34,42–47] reduce programming current, and can simultaneously improve reliability.[38,42,43]

In 2003, Lai[17] highlighted cell physics, programming current reduction, and high-density manufacture as the key areas of development needed for the widespread success of PCM. Hudgens and Johnson[48] emphasized similar points in their review outlining the history, fundamental physics and device operation, and recent technological progress in

TABLE 1: Electrical and thermal properties of the phase change material GST. These properties will vary from sample to sample. The values shown here provide only an idea of the expected values of these properties. The Debye temperatures are calculated using the number density and sound velocities of each phase, with the supplied references offering additional estimates, ∼300 K. The values for k represent those shown in Fig. 7. The values for S represent room temperature data for 380 nm– and 550 nm–thick GST, with the larger values corresponding to thinner samples.[90] The variability in ZT, evaluated at room temperature, is due to the range of values in k, S, and σ

Phase \ Property	a-GST	f-GST	h-GST
$v_{p,l}$ (m s^{-1}) (Ref. 61)	2250	3190	3300
ρ (g cm^{-3}) (Ref. 16)	5.9	6.3	6.4
C (J Kg^{-1} K) (Refs. 2 and 118)	170–202		
θ_D (K) (Refs. 38, 61, and 87)	210	250	370
k (W m^{-1} K^{-1})	0.14–0.29	0.29–0.95	0.77–2.14
k_p (W m^{-1} K^{-1}) (Ref. 61)	0.27	0.40	0.42
k_e (W m^{-1} K^{-1}) (Ref. 61)	0.000024	0.015–0.07	1.1
σ (Ω^{-1} cm^{-1}) (Ref. 61)	0.033	22–99	1709
S (mV K^{-1}) (Refs. 5 and 90)	0.43–0.55	0.28–0.38	.036
ZT (Refs. 5 and 90)	6–21 × 10^{-4}	0.06–1.47	3–9 × 10^{-4}

PCM. These authors[48] observe that the earliest devices[12,14] suffered from excessive programming currents due to poor thermal efficiency, which was first addressed nearly three decades later. A 2005 perspective[49] emphasized the contribution of Lankhorst[50] to reducing switching power and time through thermal design and use of new PC materials. Wuttig and Yamada[51] prepared a comprehensive review of PC material modeling and measurements and suggested that understanding the interplay between thermal and electronic conduction in the crystalline state is essential to overcoming this hurdle. Most recently, Lacaita et al.[52] reviewed PCM simulations and suggested that there is a need for additional study of electrical transport phenomena.

This chapter reviews thermal transport physics in phase change memory materials relevant for high-density data storage applications. We refer the reader to reviews of nanoscale thermal transport physics,[53] thermometry,[54] and thermal boundary resistance[55,56] for a more fundamental and broad treatment of these topics. The present section focuses on recent thin film thermal measurements and the physical models critical for improving phase change data storage devices. Section 2 covers the fundamental physics involved with phase change and thermal transport in PCM devices. Section 3 focuses on experimental techniques utilized in thermal property measurements. Section 4 discusses the measured intrinsic and interface thermal transport phenomena, including topics such as the Seebeck effect, size effects, and the interplay between electrons and phonons in phase change memory materials.

2. PHASE TRANSITION MECHANISMS

Ovshinsky first described the phase change mechanism as a “rapid and reversible transition between a highly resistive and a conductive state effected by an electric field.”[11] However, there is still significant debate over whether the phase change process is electrical or thermal in nature. While Kolobov et al. showed that the phase change process between FCC and amorphous GST results from distortion of the Ge and Sb sublattices,[16] it still remains to be seen whether temperature or electric field is the driving force for phase change. The phase change mechanism may be a combination of both processes, with their respective degrees of contribution depending on the specific switching technique in use.

Although initially switched using electric fields,[11] subsequent work demonstrated the use of optical[57−60] and thermal[29,61] phase change methods. In the case of an applied electric field, a current filament sets up through the phase change medium.[62,63] Joule heating within this filament causes the local temperature to rise rapidly. If this temperature exceeds the melting or crystallization temperature of the phase change material and the material is subsequently quenched, the heated region switches to the amorphous or crystalline phase. The switching times, temperatures, and currents involved in this process are crucial limiting factors in the device figure of merit. These properties are affected by local phase content,[64−66] film thickness,[66,67] stoichiometry,[68,69] and thermoelectric properties.[70,71]

In the case of optical switching, if sufficient photon energy flux is incident on the phase change material, the absorbed energy will result in a temperature excursion in the pumped area that induces phase change. This technique, commonly used for CD-RW drives, is

thermal in nature. However, Dresner and Stringellow demonstrated phase transformations using high-energy optical pulses without exceeding the crystallization temperature.[72] The wavelength dependence of the observed transition further demonstrated that phase transformation depended on the number of electron-hole pairs created by the influx of optical energy. Later experiments confirmed the nonthermal nature of optical phase change using ultrafast laser pulses.[73,74] Konishi et al.[73] were able to switch $Ge_{10}Sb_2Te_{13}$ from crystalline to amorphous using a single 140 fs pulse from a Ti:Sapphire laser. By measuring the resulting reflectivity change over time, they confirmed that the irradiated area had transitioned to the amorphous phase within 1 ps of the application of the pulse.[73] Such a transition is on the order of the electron-phonon relaxation time in metals,[75] making it unlikely that the lattice could have reached melting temperatures. Rather, the authors suggest that the high-density electron excitation directly breaks the Ge-Te bonds in the structure, displacing the Ge sublattice.[73,76,77]

Externally applied heating, however, demonstrates that electrical current is not necessary to change the phase of a device. In the measurements of Lyeo et al.[61] and Reifenberg et al.,[29] the authors were able to induce phase change through the use of temperature-controlled ovens or hot plates. By heating the samples above the crystallization temperatures and quenching, they demonstrated the presence of FCC and HCP phases without using an electric field. Although the thermal time constant of an oven precludes the possibility of rapid phase change, structures such as those demonstrated by Lee et al.[78] offer ways to thermally switch a PCM device on timescales approaching those seen in electrical and optical switching.

2.1 Thermal Conduction Mechanisms

In the amorphous and FCC phases, thermal conduction in GST is primarily due to phonon energy transport. However, in HCP-GST, electrons contribute to thermal conduction on roughly the same order as phonons. This added contribution to thermal conduction affects not only the intrinsic resistance of the film, but the thermal boundary resistances (TBRs) as well. Existing models for TBR rely on the principle of acoustic[79] or diffuse[55] reflection of phonons at a material interface. There are theories that expand these models to include both electron and phonon conduction,[80,81] but these models operate on the assumption that one of the materials involved restricts electron heat transfer.[81] In the case of a PCM device, in which HCP-GST is in contact with an electrically conductive electrode, such theories may be insufficient for estimating TBR.

The acoustic properties of FCC- and HCP-GST do not differ to a great degree, with the densities,[82] volumetric heat capacities,[83] and longitudinal phonon velocities[61] of the two phases differing by $<3\%$. Further, due to the high degree of material disorder in GST, the phonon mean free path (MFP) (<1 nm) is significantly less than the average grain size (20–30 nm).[84] As a result, grain growth does not significantly affect the average phonon MFP. Using the minimum thermal conductivity model, one can determine the expected phonon contribution to conduction in such materials. The minimum thermal conductivity model for amorphous solids describes thermal transport as a random walk of energy between localized oscillators.[61,85] In the high-temperature limit under the Debye approximation

for phonon dispersion, it predicts no temperature dependence of the lattice component according to

$$k_{\min} = \frac{1}{2}\left(\frac{\pi}{6}\right)^{1/3} K_{\mathrm{b}} n^{2/3} \left(v_{\mathrm{l}} + 2v_{\mathrm{t}}\right) \quad (1)$$

where K_{b} is the Boltzmann constant, n is the atomic number density, and v_{l} and v_{t} are the longitudinal and transverse phonon velocities, respectively. Assuming constant or increasing heat capacity and MFP, both models demonstrate that the increases in the sound velocity from the amorphous to the FCC phase[61,86] should contribute to an increase in lattice conductivity. However, it is unlikely that the phonon thermal conductivity differs significantly between FCC- and HCP-GST. The difference in thermal conductivity between the two phases of crystalline GST instead comes from a dramatic increase in the hole concentration and mobility in HCP-GST, greatly increasing electrical conductivity.[61] The Wiedemann-Franz-Lorenz (WFL) rule allows us to relate the electron contribution to thermal conductivity, k_{e}, to the electrical conductivity, σ, using the relation

$$\frac{k_{\mathrm{e}}}{\sigma} = L_{\mathrm{WFL}} T \quad (2)$$

where T is ambient temperature and the proportionality constant L_{WFL} is the Lorenz number, 2.45×10^{-8} W Ω K^{-2}. This rule applies in situations when the relaxation times for charge and heat transport are similar. This occurs when the material temperature is greater than half the Debye temperature, or less than approximately 10 K. In the intermediate range, electron-phonon scattering affects charge transport more than thermal transport. Since, as Table 1 shows, the Debye temperature of GST is ~300 K,[87] the WFL is an appropriate tool for estimating electron thermal conductivity. This results in an expected electron thermal conductivity contribution accounting for ~75% of the total thermal conductivity of HCP-GST (Fig. 3).

Phonons play an important role in thermal transport in PC and many electrode materials such as TiN.[88] The role of electrons is not fully understood in phase change materials such as GST. In electrode materials such as TiN, the electron contribution to the thermal conductivity depends on the material choice and process conditions.[32,88,89] In the molten

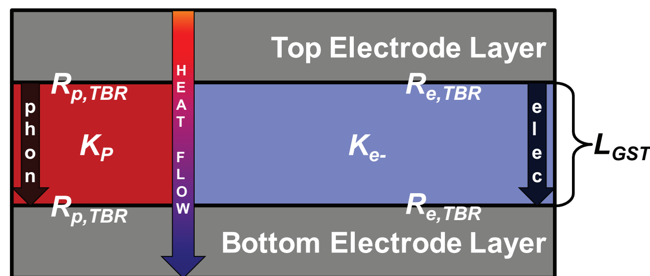

FIG. 3: The left and right regions indicate the relative contributions of phonons and electrons, respectively, to thermal conductivity in HCP-GST. The relative sizes of the regions indicate the proportions of thermal conductivity due to phonon and electron conduction. The phonon and electron components of TBR are indicated.

phase, the electrical resistivity of GST is comparable to that in the HCP phase,[90] so electrons probably play an important role in thermal transport[61] during reset pulses. In general, the thermal interface transport in PCM devices involves phonon-phonon, electron-phonon, and electron-electron processes (Fig. 4). Many devices leverage TBR to reduce the programming current[38–41,91] and improve reliability.[38] The following section summarizes the physical models of TBR and critical results important for improving PCM devices.

2.2 Thermal Boundary Resistance Mechanisms

Thermal boundary resistance arises from the incomplete transmission of heat carriers across an interface.[55,56] The ratio of the temperature discontinuity, ΔT, across an interface to the heat flux, q'', defines the boundary resistance,

$$R_{\mathrm{b}} \equiv \frac{\Delta T}{q''} \tag{3}$$

Pollack[56] and, later, Swartz and Pohl[55] prepared comprehensive reviews of TBR modeling and measurements for liquid-solid and solid-solid interfaces. Recent work offers insight into the classical mismatch models,[92–96] high-temperature TBR,[97] metal-nonmetal TBR,[81,89,98,99] and metal-metal TBR.[100] In this context, the term metal applies to materials in which electrons contribute significantly to thermal transport, while phonons dominate

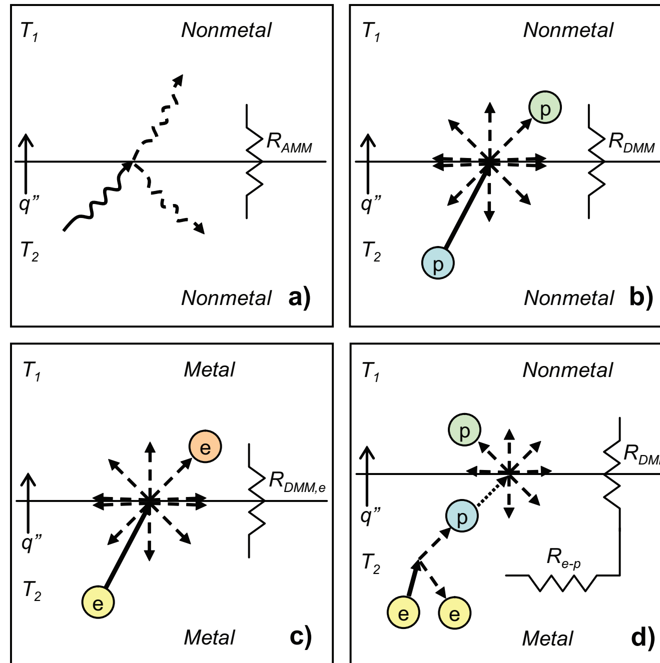

FIG. 4: Physical depictions of several TBR models: (a) acoustic mismatch model (AMM);[55] (b) diffuse mismatch model (DMM);[55] (c) electron DMM;[100] (d) electron-phonon coupling model.[81] The e and p denote electrons and phonons, respectively.

thermal transport in nonmetals. There is an abundance of TBR models, but the search for a quantitatively accurate model that applies for a wide range of materials and temperatures is a topic of ongoing research. Nevertheless, many of the models offer physical insight that can be applied to improving PCM design.

2.3 Nonmetal-Nonmetal TBR

The two most common analytical models for TBR are the acoustic mismatch (AMM) and diffuse mismatch (DMM) models.[55,92,101] These models predict interfacial phonon transmission and reflection rates, which dominate the thermal resistance at nonmetal interfaces. The AMM treats the TBR using a continuum acoustics model that describes phonon transmission by the mismatch in acoustic impedances. Transmission obeys an analog to Snell's law, and reflections are specular. The AMM finds agreement with experimental data for many interface combinations at temperatures less than 10 K.[55] The DMM better predicts TBR at higher temperatures by assuming diffuse phonon scattering at the boundary. Figures 4(a) and 4(b) show schematics of the AMM and DMM models, respectively, at nonmetal interfaces. TBR scales in inverse proportion to the transmission coefficient, α_{1-2}, given by

$$a_{1\to 2} = \frac{\sum_j c_{2,j}^{-2}}{\sum_j c_{1,j}^{-2} + \sum_j c_{2,j}^{-2}} \tag{4}$$

for the DMM model, where $c_{i,j}$ refers to the sound velocity in material i in phonon mode j.[55] Equation (4) qualitatively describes the phonon density of states (DOS) mismatch between materials 1 and 2. Materials with large DOS mismatches generally have larger TBRs.[98] The Debye temperature ratio offers another estimate of the DOS mismatch.[38,98] Modified approaches based on the AMM and DMM attempt to improve agreement with experiments by capturing a range of physical effects such as the actual weak bonding at the interface[93] and the actual DOS.[92] The latter method accounts for the actual DOS through the measured volumetric heat capacity of the film, $c_1(T)$. This value is used to extract TBR via

$$R_{\mathrm{b}} = \left(\frac{a_{1\to 2}}{12} c_{1\mathrm{D}}^3 \sum_j c_{1,j}^{-2} \right)^{-1} c_1(T)^{-1} \tag{5}$$

where the subscript D refers to the use of the Debye model and the assumption that all phonon polarizations have the same sound velocity. Molecular dynamics simulations offer detailed explanations of several other influential effects: the frequency dependence of the transmission coefficient,[94] phonon transmission between dissimilar lattices,[96] the role of anharmonic effects in the temperature dependence,[97] and the effect of interface disorder.[95,97]

2.4 Metal-Metal Thermal Boundary Resistance

When electrons contribute significantly to the thermal conductivity of one or both contacting materials, they also affect interfacial transport. In the case of metal-metal interfaces,

electrons dominate thermal transport in both materials. The TBR at metal-metal interfaces is about an order of magnitude smaller than that when a nonmetal is involved.[100] Mahan and Bartkowiak[80] showed boundaries have an exact analog for the WFL rule,

$$R_{\text{b,WFL}} = \frac{\rho_{\text{b}}}{LT} \tag{6}$$

where ρ_{b} is the electrical boundary resistance (EBR) in $\Omega\ \text{m}^2$. This result applies to interfaces such as grain boundaries, where the contacting materials are identical. Gundrum et al.[100] derived a DMM model for TBR between different metals,

$$R_{\text{DMM,e}} = \frac{4\left(Z_1 + Z_2\right)}{Z_1 Z_2} \tag{7}$$

where $Z_i = \gamma_i T v_{\text{f},i}$ is the product of the electronic heat capacity per unit volume, $\gamma_\iota T$, and the Fermi velocity, $v_{\text{f},i}$, of side i, and γ_ι is the Sommerfeld parameter. Figure 4(c) schematically depicts the electron DMM model, which shows relatively good agreement with experimental data for Al/Cu interfaces.[100] Given the intimate relationship between charge and thermal transport at metal-metal contacts, *in situ* characterization of the EBR could provide much insight into the high-temperature TBR in PCM devices.

2.5 Metal-Nonmetal Thermal Boundary Resistance

The electron and phonon systems must interact to transport heat across metal-nonmetal boundaries. Huberman and Overhauser[99] and, later, Sergeev[102] showed electrons exchange energy anharmonically with joint phonon states near the interface. The joint phonon states subsequently communicate energy between the materials. Majumdar and Reddy[81] showed that electron-phonon coupling in the bulk of the metal, followed by phonon-phonon transmission at the interface, can also contribute significantly to the metal-nonmetal TBR. Figure 4(d) shows this scenario schematically. The additional resistance contribution from the electron-phonon coupling, $R_{\text{e-p}}$, is

$$R_{\text{e-p}} = \frac{1}{\sqrt{G k_{\text{p,metal}}}} \tag{8}$$

where G is the rate of electron-phonon energy transfer per unit volume, $\sim 10^{16}$–10^{17} W/m^3/K, and $k_{\text{p,metal}}$ is the phonon contribution to the thermal conductivity in the metal, $\sim$10–20 W/m/K.[81]

In most material interfaces, one of these mechanisms for TBR will dominate. However, in the case of a metal-GST interface, the situation is more complicated. Small device dimensions, high switching temperatures, and the unique balance between electron and phonon thermal conductivity in crystalline GST requires that all these phenomena be considered when evaluating TBR. As a result, there remains considerable work to be done on understanding the fundamental interface behavior between GST and electrode materials.

3. THERMAL PROPERTY MEASUREMENTS FOR PHASE CHANGE MATERIALS

Thin film thermal conductivity measurement techniques have grown increasingly sophisticated and relevant over the past two decades. Nanoscale thin films often have lower apparent thermal conductivities than bulk films owing to increased scattering of heat carriers at lattice defects, grain boundaries, impurities, and material interfaces. Partial heat carrier transmission at interfaces gives rise to thermal boundary resistance. In thin films, it is common for the TBR to be comparable to the intrinsic thermal resistance of the film.[53] Chalcogenide thin films, in particular, exhibit all of these effects.[29,32] A key challenge in thin film thermal property measurements is separating the intrinsic thermal resistance from the TBR.

Measurement techniques may be grouped broadly into two categories: electrical and optical methods, which refers to the method used for heating and thermometry. The most common electrical technique for measuring chalcogenides is the 3ω method.[103] Several studies[2,29,32,61,104–107] utilize a variety of optical methods. The characteristic time and length scales of a measurement control which thermal properties are directly accessible through the data. The measurement technique determines the scale. The measurement frequency temporally limits frequency domain electrical techniques such as the 3ω method. Various widths of 3ω structures may also be used to spatially limit the measurement and determine the anisotropic thermal properties of thin films. Detector bandwidth and laser pulse duration temporally limit optical techniques. In the equilibrium regime, the thermal diffusivity physically links the time and length scales through the relation $d_{\mathrm{char}}^2 \approx a\tau$, where d_{char} is the characteristic length, α is the thermal diffusivity, and τ is the characteristic timescale. Figure 5 illustrates this concept schematically for three common thermometry techniques: 3ω, nanosecond optical transient thermoreflectance (TTR), and optical time domain thermoreflectance (TDTR). The right axis of the figure assumes a chalcogenide thermal conductivity of 1 W/m/K. For films approximately 100 nm and thinner, the 3ω and nanosecond TTR techniques can access only spatially averaged, or effective thermal properties. These methods offer excellent sensitivity to the thin film thermal resistance, but require multiple samples and ex-post thermal models to interpret thickness dependencies of the effective thermal conductivity. In contrast, TDTR has the temporal resolution to potentially resolve the TBR and intrinsic thermal properties uniquely. This section reviews the 3ω, nanosecond TTR, and TDTR techniques, and their application to phase change memory materials.

3.1 Three Omega Technique

The 3ω method uses a microfabricated metal line as both a heater and thermometer to measure the thermal response of the underlying thin films and/or substrate.[103,108] Figure 6 depicts a typical experimental setup and sample structure for phase change memory materials. A current, I_{ω}, at frequency ω induces heat generation at frequency 2ω in the metal line. The linear thermal transfer function of the thin films and substrate relates the 2ω heating to the 2ω temperature rise in the metal line. The metal line resistance varies linearly with temperature, causing resistance oscillations, $R_{2\omega}$, at 2ω, and voltage oscillations at

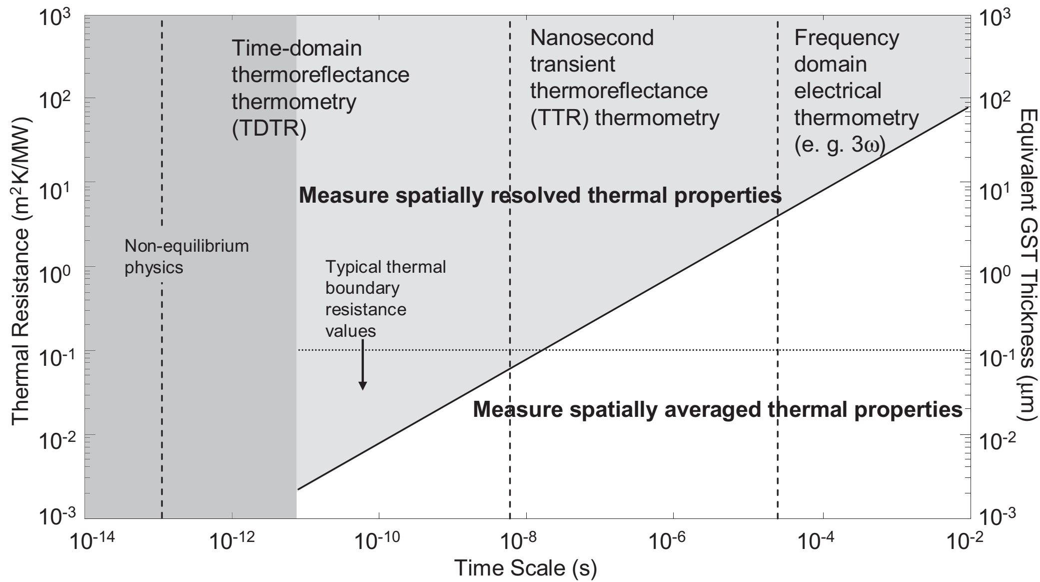

FIG. 5: A regime map detailing the characteristic length scales and timescales of different measurement techniques relevant for phase change memory materials. The equivalent GST thickness axis assumes a thermal conductivity of 1 W/m/K. The GST thickness would need to be on the order of 1–10 μm to strongly influence the frequency response in a 3ω measurement. In contrast, typical thermal boundary resistance values can uniquely influence the transient temperature profile in TDTR measurements.

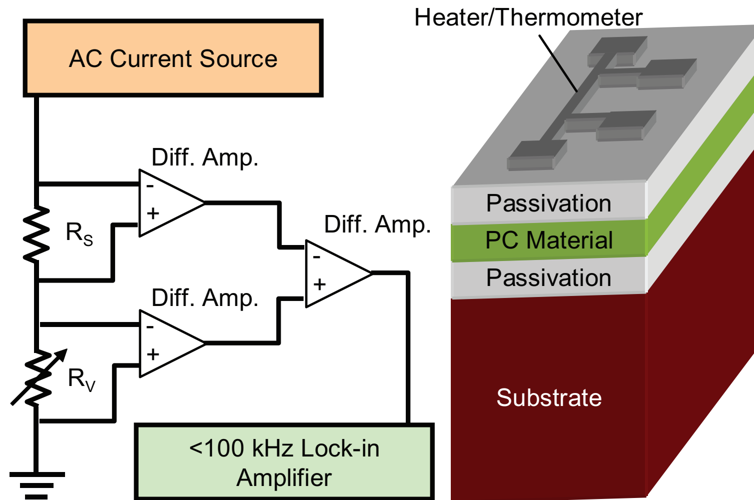

FIG. 6: Schematic of a typical 3ω setup applied to a phase change material, where R_s and R_v are static and variable resistors, respectively. Since many materials used in phase change memory are electrically conductive, passivation layers are necessary to prevent leakage current between the pads.

3ω due to the product $R_{2\omega}I_{\omega}$. A lock-in amplifier captures the 3ω voltage, which determines the thermal transfer function (i.e., thermal impedance) of the films and substrate.[103] The line heater must be completely electrically isolated to prevent measurement errors due to leakage current.[109,110] Because most phase change memory materials are electrically conductive, the PCM material is often sandwiched between passivating thin films such as SiO_2, ZnS:SiO_2, or Si_3N_4.[31,107,109–111]

Several assumptions accompany data interpretation in the 3ω method for thin films. The method directly measures the average temperature rise of the metal heater over a range of frequencies, typically 1 Hz $< f <$ 10 kHz. The thermal diffusion depth bounds the low end of the measurement frequency, which is chosen to satisfy the relations $f \gg \alpha_{\mathrm{sub}}/d_{\mathrm{sub}}^2$, and $b \ll \alpha_{\mathrm{sub}}/d_{\mathrm{sub}}^2$, where d is the substrate thickness, $2b$ is the heater width, and α_{sub} is the substrate thermal diffusivity. The limits of the lock-in amplifier and modeling errors imposed by the thermal mass of the heating element commonly limit the upper frequency range.[112] The slope of the in-phase component of the heater temperature rise versus ln(f) determines the substrate thermal conductivity.[103] The 3ω technique strictly determines the frequency-dependent thermal impedance of the thin film plus substrate.[112,113] The most common assumptions for extracting thin film properties are[83,103] (i) heat transfer through the thin films is 1D and (ii) the thermal response of the thin film is frequency independent. Combined, these assumptions permit extraction of an effective thin film thermal conductivity, k_{eff}, using the relation,[108]

$$k_{\mathrm{eff}} = \frac{Q d_{\mathrm{film}}}{2bL\Delta T_{\mathrm{film}}} \tag{9}$$

where Q is the total heating power, d_{film} is the thin film thickness, L is the heater length, and ΔT_{film} is the temperature rise exclusively across the thin film of interest, which is commonly measured differentially.[31,38] Equation (8) explains why PCM papers employing the thin film 3ω method require differential measurements. The technique measures the total temperature difference across the thin films. Extraction of ΔT_{film} requires measuring samples with and without the PCM material. Once ΔT_{film} is determined, the effective thermal conductivity contains contributions from the TBRs between the PCM and passivation materials. Studies that also vary the PCM thickness separate the TBR from the PCM material intrinsic thermal conductivity.[31,107,111] The length scales dictated by the frequency-dependent thermal penetration depth and heater widths justify Eq. (8) and expose its limitations. The primary limitation is that the spatial distribution of thermal properties is not directly accessible with this technique.

Sample geometries and data interpretation methods vary in 3ω thin film measurements. These variations may explain some of the disparity in reported thermal conductivities. Dames and Chen[113] analyzed the effect of using a voltage source, as is common, instead of a current source as assumed in the derivation of the thermal model. They show a necessary correction factor to the thermal transfer function, Z_{apparent},

$$Z_{\mathrm{true}} = Z_{\mathrm{apparent}} \left(1 - \frac{R_{\mathrm{sample}}}{R_{\mathrm{total}}}\right)^{-1} \tag{10}$$

where Z_{true} is the actual thermal transfer function to be used in fitting the data, R_{sample} is the heater resistance, and R_{total} is the total resistance of the circuit including output

impedances. It is not clear whether Dames and Chen account for the voltage source correction, or whether their respective experimental systems are insensitive to the correction factor. For a typical voltage source with an output impedance of 50 Ω, and a series resistor comparable to the heater resistance between 5 Ω and 150 Ω, the correction factor varies between 1.09 and 1.75. The extracted effective thermal conductivity underestimates the true conductivity by a similar proportion. Using low-resistance heaters or adding ballast resistors to the circuit when using a voltage source reduces the importance of the correction factor.

Heat spreading and the thermal mass of the heater introduce systematic errors to data interpretation under the 1D assumption. Risk et al.[109,110] used an optimization algorithm[112] accounting for both effects, and Fallica et al.[111] used a 3D analytical heat transfer model. Borca-Tasciuc et al.[114] examined the limits of the thin film assumptions. The ratio of the true thermal conductivity, k_{true}, to the conductivity extracted using the 1D assumptions, k_{1D}, is

$$\frac{k_{\mathrm{true}}}{k_{\mathrm{1D}}} = C_{\mathrm{dim}} S_{\mathrm{dim}} \tag{11}$$

C_{dim} and S_{dim} are nondimensional parameters given by

$$C_{\mathrm{dim}} = 1 - \frac{k_y k_x}{k_s^2} \tag{12}$$

and

$$S_{\mathrm{dim}} = (1 + 0.38\beta_{\mathrm{F}})^{-1}; \quad \beta_{\mathrm{F}} \equiv \sqrt{\frac{k_k}{k_y} \bullet \frac{d}{b}}; \quad \beta_{\mathrm{F}} < 10 \tag{13}$$

k_y, k_x, and k_s are the thin film cross-plane, thin film in-plane, and substrate thermal conductivities, respectively. The dimensional parameters d and b are the thin film thickness and heater half-width, respectively. The parameter C measures the thermal conductivity contrast between the thin film and substrate. In isotropic materials, β_{F} reduces to the ratio of film thickness to heater width. For GST and TiN films of thickness near 300 nm thick measured with 2 μm–wide heaters, the 1D assumptions contribute to approximately a 10% overestimation of the thermal conductivity. Equations (10)–(12) suggest it is possible to measure the thermal conductivity anisotropy of PCM materials by using thick films, thin heaters, thermally resistive substrates such as quartz, or suspended films.[84]

Sample design for the 3ω method involves many compromises between signal maximization, analysis complexity, and the possibility of current leakage. If using a voltage source, such as the output of a lock-in amplifier, an impedance-matched, narrow heater maximizes the measurement signal, but the corrections from Eqs. (9) and (12) may be significant. However, it has recently been suggested that voltage-driven measurements that use common mode subtraction do not require the correction factor.[115] In either case, using a current source always circumvents the need for Eq. (9) and the associated design trade-offs. Pinholes in the passivation layer or punctures from probes or wirebonds can cause current leakage through the PCM material. Increasing the passivation layer thickness can help prevent puncturing, but reduces the sensitivity to the PCM thermal conductivity. Increasing the heater thickness can also prevent puncturing, but the additional thermal mass may

affect the measurement at high frequencies.[114] Risk et al.[110] recommend using beryllium-copper probe tips and advise against a wide variety of other contact methods. The need for electrical contact also complicates high-temperature measurements.[110] Ultimately, leakage current characterization is essential for guaranteeing the reliability of 3ω measurements of thin films containing conducting materials.

Several authors report the thermal conductivity of PCM materials using the thin film 3ω method, summarized versus film thickness in Fig. 7.[29−32,61,78,83,87,107,109−111,116−120] Kim et al.[31] report the amorphous and FCC phase GST intrinsic conductivity and ZnS:SiO2/GST TBR between 50 and 300 K using multilayer samples. Giraud et al.[83] measured effective thermal conductivities for ZnS:SiO2, SiO2, amorphous GST, FCC-GST, and TiN. Risk et al.[109] developed an *in situ* 3ω technique to monitor the effective thermal conductivity of GST during the amorphous to FCC phase transition. Risk et al.[110] subsequently measured the effective thermal conductivities of the phase change materials GST, N-doped GST, AgInSbTe alloy, and GeSb, suggesting a modified Wiedemann-Franz law to predict the temperature dependence of the thermal conductivity. Fallica et al.[111] report the room temperature thermal conductivity of SiO_2, Si_3N_4, amorphous, FCC, and HCP-GST, and the SiO_2/GST TBR. Lee et al.[107] used a combination of optical and 3ω techniques to report the thermal conductivity of various thicknesses of a-GST and FCC-GST thin films, along with the thermal boundary resistance betweens these films and Si_3N_4 passivation layers. A microthermal stage, developed by Lee et al.,[78] was used to simultaneously characterize

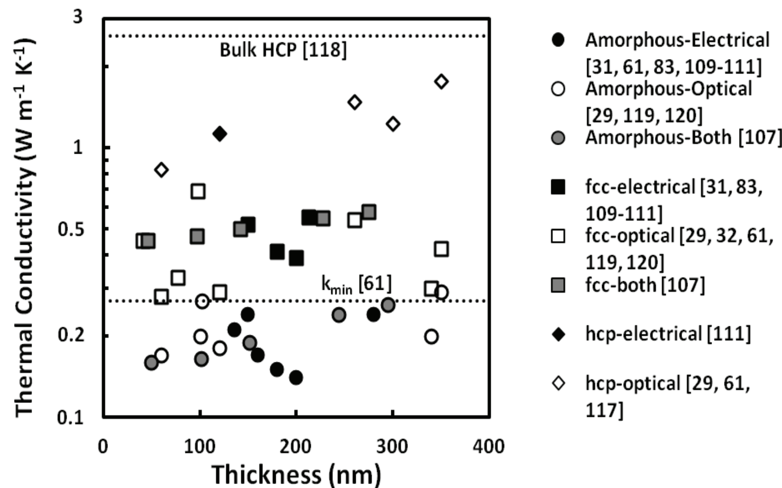

FIG. 7: Thickness dependence of the effective and intrinsic thermal conductivities for $Ge_2Sb_2Te_5$ at room temperature in the amorphous (λ), FCC (ν), and HCP (τ) phases. Solid markers indicate 3ω measurements. Open markers indicate optical measurements. Gray markers indicate that both optical and electrical techniques were performed. For 3ω and optical measurements using multiple thicknesses, we plot the extracted intrinsic conductivity at the location of the average sample thickness. The horizontal line labeled $k_{\min}$ indicates the minimum thermal conductivity estimate in the amorphous phase,[61] and the horizontal line at the top is the bulk thermal conductivity measured in the HCP phase.[118]

and control the temperature of thin GST films. The authors used this technique to locally cycle GST between the SET and RESET states, and measure the resulting electrical and thermal conductivity. Lee et al.[121] also utilized in-plane steady state electrical thermometry on suspended GST thin films to determine in-plane thermal properties, demonstrating significant anisotropy due to phase impurities in the film. Li et al.[122] confirmed the effect of phase impurities on lateral thermal conduction, and suggested the use of such to reduce the programming current of lateral PCM devices by up to 30%.

3.2 Photothermal Property Measurements

Optical thermometry techniques for PCM materials measure the transient change in reflectance to probe the thermal response of a thin film stack. In contrast to the 3ω technique, optical techniques are noncontact and do not require electrical passivation layers or microfabrication steps beyond blanket film deposition. These features make optical techniques preferable to electrical techniques when conducting temperature-dependent measurements. However, data extraction in optical thermometry often requires a numerical solution of the heat diffusion equation, and it is significantly more challenging to measure the absolute temperature. Absolute optical temperature measurements require careful calibration of the temperature-dependent reflectance, absorbed laser power, and photodiode responsivities.[123] These steps are unnecessary in linear thermal systems, where the shape alone of the transient thermal response determines the thermal properties.

The first optical measurements[2,104,105,124] used the phase-dependent reflectance changes in optical PC disks to probe their thermal properties. A multiparameter fitting routine matches the reflectance data to simulations of the coupled heat diffusion, phase change, and optical processes.[2,104,124] Recent optical measurements use nanosecond TTR[29,87,107,116,117,120] and TDTR.[32,61] These techniques offer improved sensitivity and reduced errors due to systematic experimental errors compared to other optical methods.[30] In thermoreflectance measurements, a high-intensity laser pulse (i.e., pump) causes a temperature excursion in the sample. A probe beam samples the temperature of a metal transducer via its relative reflectance change. Due to the linearity of the heat diffusion and transducer reflectance variation with temperature, thermal property data can generally be extracted without knowledge of the absolute temperature magnitude. A wide range of materials satisfy the linearity requirements, making thermoreflectance a robust choice for thermal property measurements. This section focuses on thermoreflectance measurements of PCM materials.

3.3 Nanosecond Transient Thermoreflectance

Nanosecond TTR systems measure thermal decays in the range of tens of nanoseconds to tens of microseconds with temporal resolution <10 ns.[125,126] The reflected intensity of a continuous wave (CW) probe laser interrogates the transient surface temperature of a metal transducer via a high-speed photodiode. TTR systems used in PCM material measurements have two common configurations: dual transducer[87,116,117] and single transducer.[29,30,120,126] In a dual-transducer system, two metal layers sandwich the thin

film or films of interest. The pump and probe beams strike opposing sides of the sample, which is similar in principle to bulk flash diffusivity measurements.[127] The substrate must be transparent at the pump or probe wavelength. Figure 8 depicts a typical single-transducer TTR system.[29,30,120,126] A single-metal layer coating the thin film of interest serves as both the pump absorber and probe transducer. When the thermal mass of the metal transducer is large, this configuration benefits from decreased sensitivity to the heat capacity of the thin film.

The hardware in both configurations is similar. A frequency-doubled Q-switched Nd:YAG (yttrium aluminum-garnet) laser heats the sample with short (<10 ns) pulses. The photodiode typically has a bandwidth between 500 and 650 MHz.[29,119,126] The pump pulse width and photodiode bandwidth determine the maximum temporal resolution of the measurement. Samples should have characteristic thermal diffusion times longer than this to ensure measurement accuracy. A band-pass filter at the probe wavelength is essential for preventing pump leakage into the photodiode. Pump pulses recur with a frequency of ~1–10 Hz, characteristic of Q-switched lasers. The pulse repetition rate determines the maximum thermal decay time of the sample, which should be much longer than the inverse of the repetition rate to allow the sample to fully cool before the next heating event. The signal-to-noise ratio for a single pump pulse is poor, owing to the large measurement bandwidth and low transducer sensitivity. Relative reflectance changes are on the order of 10^{-4}/°C,[128] and the pump pulse typically heats the sample by <10°C.[30] Normalized thermal decay traces are, therefore, the average over thousands of heating events. The spatial extent of the pump beam is generally much larger than the thermal diffusion length, so a 1Dl, multilayer solution to the heat diffusion equation models the data.

3.4 Time Domain Thermoreflectance

TDTR is a pump-probe technique that can measure a wide range of thermal physics from electron-phonon interactions at timescales less than 10 ps to thermal decays of up to

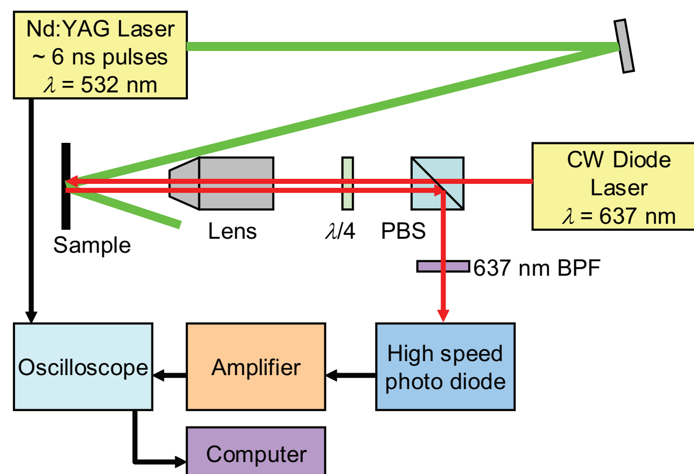

FIG. 8: Typical nanosecond TTR setup. The sample surface is a reflective metal.

7 ns.[129−131] TDTR uses a mode-locked laser to produce a pulse train with repetition rates between tens[32,131,132] and a few hundreds[129] of megahertz. Figure 9 shows one implementation of TDTR used in Refs. 32 and 132. The laser output splits between a pump beam that is often frequency doubled[32,131,132] and a probe beam that travels through a variable delay stage. The difference in optical path lengths fixes the delay time between the heating and probing events. The thermal decay trace is reconstructed by sweeping the delay stage through its range of motion. An electro-optic or acousto-optic modulator chops the pump beam, at frequencies below 100 kHz up to 10 MHz.[130] A lock-in amplifier detects the in-phase and out-of-phase components of the reflected portion of the probe beam at the modulation frequency. By limiting the measurement bandwidth to a small window around the modulation frequency, the lock-in amplifier greatly improves the signal-to-noise ratio compared to nanosecond TTR.

Several techniques can improve TDTR signal quality in practice. Capinski and Maris[133] incorporated a single-mode fiber (SMF) to reduce errors caused by probe beam misalignment and divergence as it traverses the delay stage. Schmidt et al.[131] used a beam expander to reduce beam divergence and a double pass of the delay stage to extend the measurement's temporal range. Costescu et al.[89] and Cahill[130] demonstrated that measurements of the phase ratio rather than the signal amplitude eliminate the need for pump and probe normalization and can improve the signal-to-noise ratio.

TDTR data carries a wealth of information about thin film physics. At delay times less than ∼10 ps, the two-temperature model is often used to interpret the data because the electron and lattice temperatures in the metal transducer have not equilibrated.[134] Picosecond acoustics measurements in TDTR systems can often be used to measure the local metal and thin film thicknesses and sound velocities,[61] eliminating the need for other characterization methods.[89] At longer times, various models describe the thermal decays, the

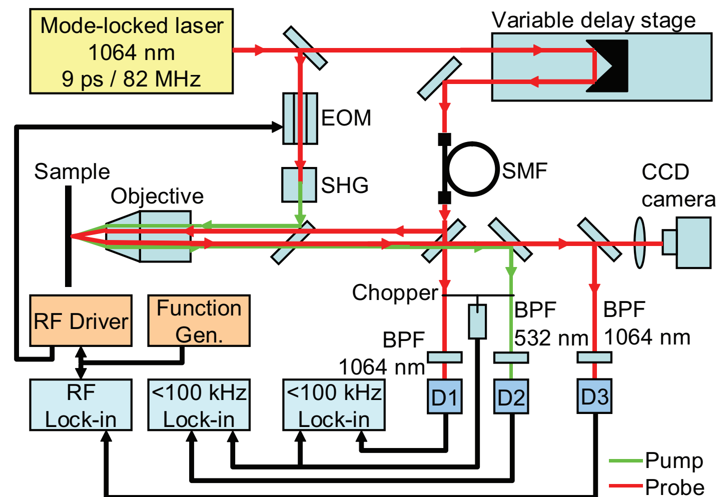

FIG. 9: One implementation of a picosecond TDTR setup.[32,132] Other implementations use a Ti:sapphire laser and the phase ratio measured by the RF lock-in,[130,131] but the systems are similar in principle.

most general being a 3D, multilayer, frequency domain solution to the heat diffusion equation accounting for radial spreading and pulse accumulation.[32,130,131] Schmidt et al.[131] suggested varying the modulation frequency to sample different thermal properties, while Reifenberg et al.[32] recently used a series of different sample geometries to simultaneously extract intrinsic thermal properties and interface resistances. Because of its excellent temporal resolution, TDTR can directly measure TBR.[89,132] Although the advantages of TDTR are numerous, the experimental apparatus and data analysis are considerably more complex than nanosecond TTR and 3ω.

4. THERMAL PROPERTY MODELING AND MEASUREMENTS IN PCM MATERIALS

Figure 10 summarizes the temperature-dependent amorphous, FCC, and HCP phase thermal conductivities of GST reported using nanosecond TTR and TDTR. For clarity, the figure does not show effective conductivity data for the 350 nm and 60 nm layers measured in Ref. 29. Including 3ω and effective thermal conductivity measurements, the amorphous, FCC, and HCP thermal conductivities span the ranges 0.14–0.29 W/m/K, 0.29–0.95 W/m/K, and 0.77–2.14 W/m/K, respectively. Several studies note that mass diffusion,[117] phase change material sublimation,[29,32] and component failure[109] limit the peak measurement temperature to 350–400°C. Overcoming these challenges to measure thermal properties up to and beyond the melting temperature remains an important goal.

The differences between amorphous phase measurements are generally small. Because amorphous materials conduct heat through a network of localized oscillators,[61,85] it is likely that structural defects do not strongly affect the thermal conductivity. The differences in the measured amorphous phase thermal conductivity may instead be due to partial

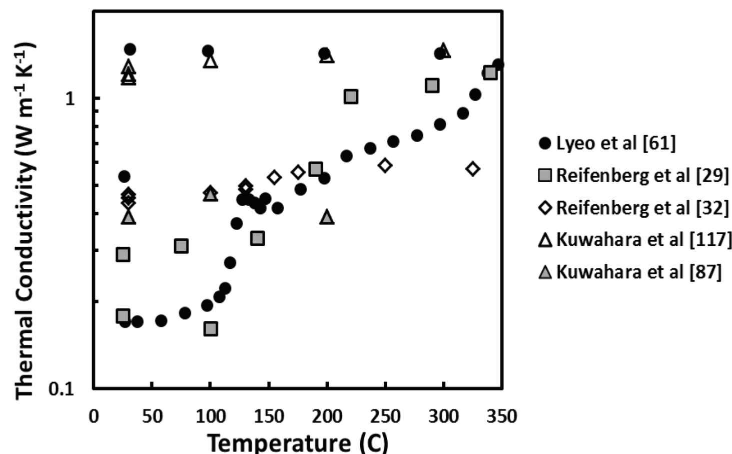

FIG. 10: Temperature-dependent thermal conductivity data for $Ge_2Sb_2Te_5$ taken with optical measurement systems. The data from Ref. 29 are for a 120 nm layer that underwent the FCC-to-HCP phase transition just above 200°C, as opposed to ~340°C for the sample in Ref. 61.

crystallization[30,135] and/or differences in TBR in the case of effective thermal conductivity measurements.

The room temperature FCC phase conductivity generally falls between 0.3 W/m/K and 0.57 W/m/K. Measurements show that increases in the electron contribution[110] and lattice contribution[61] can both account for the larger FCC phase thermal conductivity. The temperature dependence of the FCC phase conductivity is particularly important because it may strongly influence the programming current.[33,34,136] Lyeo et al.[61] show increasing FCC thermal conductivity with temperature. Other studies report no temperature dependence,[87] or a slower increase in the FCC thermal conductivity with temperature.[29,32]

Most thin film HCP thermal conductivity measurements span the range 1–2 W/m/K. The HCP phase exhibits an approximately 10-fold to 100-fold decrease in electrical resistivity[61,90,137] attributed to increased hole mobility.[61] Unlike the FCC and amorphous phases, the electrical resistivity increases with temperature.[90] The electron contribution dominates the HCP phase conductivity.[61,117,118,138]

4.1 Electron Thermal Conductivity

Despite the FCC phase having $\sim 10^3$–10^4 times higher electrical conductivity than the amorphous phase,[90,137] the increased electron contribution does not explain the differences in thermal conductivity in all measurements. At room temperature, the WFL predicts a small electron contribution in the FCC phase in Ref. 61 that does not fully account for the difference in FCC and amorphous thermal conductivities. Risk et al. confirm that the electron contribution does not explain the difference.[109,110] At 300°C, assuming an activation energy of 0.14 eV[34,90] and constant lattice conductivity,[61] the WFL overestimates the measured temperature dependent in FCC thermal conductivity.[61,32,87] The WFL alone cannot explain the observed temperature dependence of the FCC phase thermal conductivity. Simultaneous temperature-dependent electrical and thermal conductivity measurements could offer insight into the role of electrons in thermal transport in the FCC phase.

4.2 Lattice Thermal Conductivity

Molecular dynamics simulations accounting for anharmonic effects may improve understanding of lattice conduction, including its temperature dependence. Reifenberg et al.[29] suggested that the microstructure plays an important role in reducing the effective thermal conductivity. In crystalline materials with long-range order, defects act as phonon scattering sites, reducing the intrinsic thermal conductivity.[53] The relative importance of the microstructure contribution decreases during and after annealing.[29,61] Although no studies have directly examined their role, deposition conditions may strongly impact the microstructure. Annealing experiments with variable time and temperatures can also improve understanding of the lattice contribution to the thermal conductivity.

4.3 Thermal Boundary Resistance in Phase Change Materials

There are limited TBR data for PCM materials. Figure 11 summarizes the available data. The TBR between the bottom electrode, or heater, and the GST is extremely important

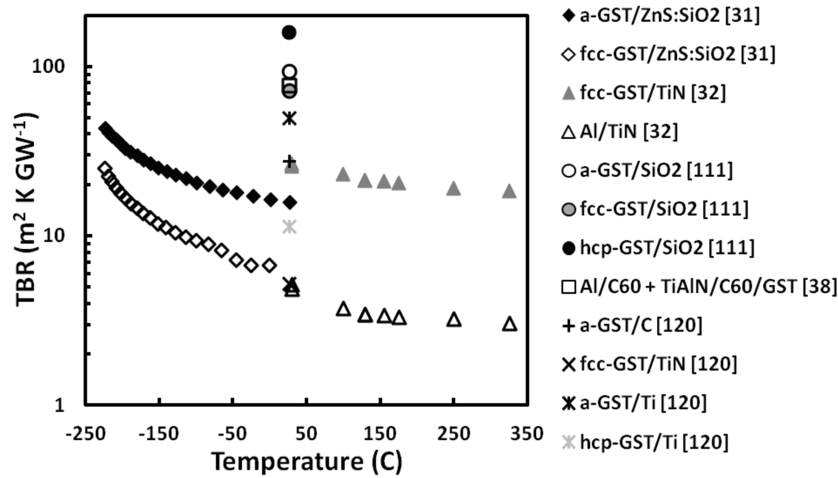

FIG. 11: Summary of the temperature-dependent thermal boundary resistance data for phase change materials. A TBR of 10 m^2K/GW has thermal resistance equal to $\sim$190 nm of TiN,[32] or 14 nm of thermally grown SiO_2.

since the bottom electrode dissipates most of the heat during programming.[136] The TiN/FCC GST TBR decreases from 26 m^2K/GW to 19 m^2K/GW between 30°C and 325°C.[32] A TBR of 10 m^2K/GW is equivalent in thermal resistance to $\sim$190 nm of TiN at room temperature,[32] or $\sim$14 nm of thermally grown SiO_2. At room temperature, the series combination of the TiN/GST TBR and Al/TiN TBR increases the apparent thermal resistance through the heater by almost a factor of seven, assuming a 100 nm-tall TiN heater contacted by an Al interconnect[32] Kim et al.[38] showed an even larger average interface resistance of $\sim$77 m^2K/GW between a C_{60} layer, used as part of the bottom electrode, and Al and TiAlN films. The results for these electrode materials agree qualitatively with other materials with similar Debye temperature mismatches.[98] Other studies used the 3ω method to extract the TBRs between GST and ZnS:SiO_2,[31] an important interface in optical media, and GST and SiO_2.[111] Both reports show larger TBR in the amorphous phase, which the authors attribute to larger acoustic mismatch and interface roughness. Reifenberg et al.[32] reported that the application of the DMM using the measured heat capacity[92] yields predictions that best match the temperature-dependent data for phonon-dominated TiN/FCC GST TBRs.

The TBR models and data raise many questions whose answers will improve PCM design and engineering. The models demonstrate that the nature of charge and thermal transport in the electrode and phase change material play an essential role in determining the TBRs. The temperature-dependent transport properties of thin film electrode materials such as TiN are not well characterized. The intrinsic electrical properties of GST are well understood, but the EBR is not. High-temperature TBR measurements of GST thin films at $T > 400$°C still pose significant challenges for standard experimental approaches. Ptitsina et al.[139] showed that transverse phonons dominate electron-phonon coupling in impure thin metal films over a wide temperature range. Because the molten phase does

not support transverse modes, the high-temperature TBR may not conform to the standard models.

4.4 Thermoelectric Transport

As temperature gradients increase in scaled devices, thermoelectric effects may become increasingly important. A recent study[25] attributes programming asymmetry in a linear PCM cell to thermoelectric effects. Suh et al.[70] used electrothermal simulations to demonstrate that, by carefully selecting PCM electrode materials based on Seebeck coefficient, thermoelectric heating can significantly reduce programming current. Lee et al.[140] recently developed SOI structures to characterize the thermoelectric power generated at such interfaces, specifically for TiW-SbTe.

The low thermal conductivity and small band gap in phase change materials makes them excellent candidates as thermoelectric materials.[141] Ohta et al.[90] showed that the room temperature Seebeck coefficients of thin GST in the amorphous and FCC phases are comparable to those in the best thermoelectric materials.[7,142] Further complicating matters is the existence of the boundary Seebeck effect,[143] and its temperature dependence. The possibility of using phase change nanowires,[20–22,35] nanotubes,[144] and nanoparticles[23,145] to minimize device size merits investigation of their thermal properties. Lee et al.,[146] for example, reported low effective thermal conductivities for GST-SiO_2 thin film composites. Ryu et al.[71] later showed that such composites reduce reset current by up to 45% from pure GST. Use of vertically aligned Ge nanowires[24] or carbon nanotubes as the heater can significantly reduce the device cross-sectional area. The possibility of ballistic transport in these structures further complicates thermal conductivity and TBR calculations, but may significantly reduce programming current.[70]

4.5 Commentary on Thermal PCM Research

The goals of reducing programming current and cell dimensions in PCM devices remain driving forces for research into the thermal properties of phase change materials. However, the vast body of literature shown here demonstrates that the intricate thermal physics of these materials are fascinating enough on their own to merit study. It has been almost 45 years since phase change materials were first demonstrated, and we are still answering many fundamental questions about their physical behavior. Certain phases of PCM have similar electron and phonon contributions to thermal conductivity, inviting study into electron-phonon coupling effects in both bulk GST and GST-electrode/dielectric interfaces. Such studies may be the route to a more generalized understanding of electron-phonon interaction in TBR. The desire to understand electrothermal phenomena in phase change materials has inspired the development of novel measurement techniques of interest to the microscale heat transfer community, with many more likely in the pipeline. Low GST band gap and low thermal conductivity make it a promising thermoelectric material. Interface engineering and nanostructuring may further increase the figure of merit. These projects are capable of standing on their own merits, and need not run under the auspices of building a better PCM cell. Their results, however, will remain critical to the PCM community.

REFERENCES

1. E. Small, Y. Yang, S. M. Sadeghipour, and M. Asheghi, Simulation of the writing on the patterned optical phase-change recording media, *J. Appl. Phys*., **99**(3):033101, 2006.
2. C. Peng, L. Cheng, and M. Mansuripur, Experimental and theoretical investigation of laser-induced crystallization and amorphization in phase-change optical recording medi, *J. Appl. Phys*., **82**(9):9, 1997.
3. S. Lai and T. Lowrey, OUM—A 180 nm nonvolatile memory cell element technology for stand alone and embedded applications, *International Electron Devices Meeting, IEDM Technical Digest*, pp. 36.5.1–36.5.4, 2001.
4. A. Pirovano, A. L. Lacaita, A. Benvenuti, F. Pellizzer, S. Hudgens, and R. Bez, Scaling analysis of phase-change memory technology, *IEEE International Electron Devices Meeting, 2003. IEDM '03 2003 Technical Digest*, pp. 29.6.1–29.6.4, 2003.
5. F. Yan, T. J. Zhu, X. B. Zhao, and S. R. Dong, Microstructures and thermoelectric properties of GeSbTe base layered compounds, *Appl. Phys. A*, **88**(2):425–428, 2007.
6. P. P. Konstantinov, L. E. Shelimova, E. S. Avilov, M. A. Kretova, and V. S. Zemskov, Thermoelectric properties of $nGeTe \cdot mSb_2Te_3$ layered compounds, *Inorg. Mater*., **37**(7):662–668, 2001.
7. J. D. Koenig, H. Boettner, J. Tomforde, and W. Bensch, Thermoelectric properties of phase-change materials, *26th International Conference on Thermoelectrics*, pp. 390–393, 2007.
8. M. LaPedus, Samsung to ship MCP with phase-change, *EE Times*, 2010.
9. P. Clarke, ISSCC: Samsung preps 8-Gbit phase-change memory, *EE Times*, 2011.
10. J.-B. Park, G.-S. Park, H.-S. Baik, J.-H. Lee, H. Jeong, and K. Kim, Phase-change behavior of stoichiometric $Ge_2Sb_2Te_5$ in phase-change random access memory, *J. Electrochem. Soc*., **154**(3):H139–H141, 2007.
11. S. R. Ovshinsky, Reversible electrical switching phenomena in disordered structures, *Phys. Rev. Lett.*, **21**(20):1450–1455, 1968.
12. R. G. Neale, Device structures and fabrication techniques for amorphous semiconductor switching devices, *J. Non-Cryst. Solids*, **2**:558–574, 1970.
13. R. G. Neale and J. A. Aseltine, The application of amorphous materials to computer memories, *IEEE Trans. Electron Devices*, **20**(2):195–205, 1973.
14. D. L. Nelson, Ovonic device applications, *J. Non-Cryst. Solids*, **2**:528–539, 1970.
15. A. M. Gibby, A layered chalcogenide phase change memory device, *Electrical Engineering*, Stanford University, Stanford, p. 203, 2008.
16. A. V. Kolobov, P. Fons, A. I. Frenkel, A. L. Ankudinov, J. Tominaga, and T. Uruga, Understanding the phase-change mechanism of rewritable optical media, *Nat. Mater*., **3**(10):703–708, 2004.
17. S. Lai, Current status of the phase change memory and its future, *IEEE International Electron Devices Meeting, IEDM '03 Technical Digest*, pp. 10.1.1–10.1.4, 2003.
18. F. Bedeschi, R. Fackenthal, C. Resta, E. M. Donze, M. Jagasivamani, E. Buda, F. Pellizzer, D. Chow, A. Cabrini, G. M. A. Calvi, R. Faravelli, A. Fantini, G. Torelli, M. Duane, R. Gastaldi, and G. Casagrande, A multi-level-cell bipolar-selected phase-change memory, *IEEE International Solid-State Circuits Conference, Digest of Technical Papers*, pp. 428–625, 2008.

19. C. W. Jeong, D. H. Kang, D. W. Ha, Y. J. Song, J. H. Oh, J. H. Kong, J. H. Yoo, J. H. Park, K. C. Ryoo, D. W. Lim, S. S. Park, J. I. Kim, Y. T. Oh, J. S. Kim, J. M. Shin, J. Park, Y. Fai, G. H. Koh, G. T. Jeong, H. S. Jeong, and K. Kim, Writing current reduction and total set resistance analysis in PRAM, *Solid-State Electron.*, **52**(4):591–595, 2008.

20. S. Meister, H. Peng, K. McIlwrath, K. Jarausch, X. F. Zhang, and Y. Cui, Synthesis and characterization of phase-change nanowires, *Nano Lett.*, **6**(7):1514–1517, 2006.

21. S.-H. Lee, Y. Jung, and R. Agarwal, Highly scalable non-volatile and ultra-low-power phase-change nanowire memory, *Nat Nano*, **2**(10):626–630, 2007.

22. Y. Bin, S. Xuhui, J. Sanghyun, D. B. Janes, and M. Meyyappan, Chalcogenide-nanowire-based phase change memory, *IEEE Trans. Nanotechnology*, **7**(4):496–502, 2008.

23. Y. Zhang, H. S. P. Wong, S. Raoux, J. N. Cha, C. T. Rettner, L. E. Krupp, T. Topuria, D. J. Milliron, P. M. Rice, and J. L. Jordan-Sweet, Phase change nanodot arrays fabricated using a self-assembly diblock copolymer approach, *Appl. Phys. Lett.*, **91**(1):013104, 2007.

24. S. Kim, Y. Zhang, J. P. McVittie, H. Jagannathan, Y. Nishi, and H. S. P. Wong, Integrating phase-change memory cell with Ge nanowire diode for crosspoint memory; experimental demonstration and analysis, *IEEE Trans. Electron Devices*, **55**(9):2307–2313, 2008.

25. D. T. Castro, L. Goux, G. A. M. Hurkx, K. Attenborough, R. Delhougne, J. Lisoni, F. J. Jedema, M. A. A. t Zandt, R. A. M. Wolters, D. J. Gravesteijn, M. Verheijen, M. Kaiser, and R. G. R. Weemaes, Evidence of the thermo-electric Thomson effect and influence on the program conditions and cell optimization in phase-change memory cells, *Electron Devices Meeting, IEDM 2007*, IEEE International, Washington, DC, pp. 315–318, 2007.

26. A. Majumdar, Thermoelectricity in semiconductor nanostructures, *Science*, **303**(5659):777–778, 2004.

27. X. B. Zhao, H. Y. Chen, E. Muller, and C. Drasar, Thermoelectric properties of Mn doped $FeSi_x$ alloys hot-pressed from nitrided rapidly solidified powders, *Appl. Phys. A*, **80**(5):1123–1127, 2005.

28. X. J. Zheng, L. Zhu, Y.-H. Zhou, and Q. Zhang, Impact of grain sizes on phonon thermal conductivity of bulk thermoelectric materials, *Appl. Phys. Lett.*, **87**(24):242101, 2005.

29. J. P. Reifenberg, M. A. Panzer, S. Kim, A. M. Gibby, Y. Zhang, S. Wong, H.-S. P. Wong, E. Pop, and K. E. Goodson, Thickness and stoichiometry dependence of the thermal conductivity of GeSbTe films, *Appl. Phys. Lett.*, **91**(11):111904, 2007.

30. Y. Yang H. F. Hamann, and M. Asheghi, Thermal conductivity measurements and modeling of phase-change $Ge_2Sb_2Te_5$ materials, *Nanoscale Microscale Thermophys. Eng.*, **13**(2):88–98, 2009.

31. E.-K. Kim, S.-I. Kwun, S.-M. Lee, H. Seo, and J.-G. Yoon, Thermal boundary resistance at $Ge_2Sb_2Te_5$/ZnA:SiO_2 interface, *Appl. Phys. Lett.*, **76**:3864, 2000.

32. J. P. Reifenberg, K.-W. Chang, M. A. Panzer, S. Kim, J. A. Rowlette, M. Asheghi, H.-S. P. Wong, and K. E. Goodson, Thermal boundary resistance measurements for phase-change memory devices, *IEEE Electron Device Lett.*, **31**(1):56–58, 2010.

33. U. Russo, D. Ielmini, A. Redaelli, and A. L. Lacaita, Modeling of programming and read performance in phase-change memories, Part I: Cell optimization and scaling, *IEEE Trans. Electron Devices*, **55**(2):506–514, 2008.

34. D. L. Kencke, I. V. Karpov, B. G. Johnson, L. Sean Jong, K. DerChang, S. J. Hudgens, J. P. Reifenberg, S. D. Savransky, Z. Jingyan, M. D. Giles, and G. Spadini, The role of in-

terfaces in damascene phase-change memory, *IEEE International Electron Devices Meeting*, IEEE International, Washington, DC, pp. 323–326, 2007.

35. I.-R. Chen and E. Pop, Compact thermal model for vertical nanowire phase-change memory cells, *IEEE Trans. Electron Devices*, **56**(7):1523–1528, 2009.
36. R. Warren, J. Reifenberg, and K. Goodson, Compact thermal model for phase change memory nanodevices, *11th Intersociety Conference on Thermal and Thermomechanical Phenomena in Electronic Systems*, pp. 1018–1045, 2008.
37. J. Reifenberg, E. Pop, A. Gibby, S. Wong, and K. Goodson, Multiphysics modeling and impact of thermal boundary resistance in phase change memory devices, *IEEE ITHERM 2006*, pp. 106–113, 2006.
38. C. Kim, D.-S. Suh, K. H. P. Kim, Y.-S. Kang, T.-Y. Lee, Y. Khang, and D. G. Cahill, Fullerene thermal insulation for phase change memory, *Appl. Phys. Lett*., **92**(1):013109, 2008.
39. T. C. Chong, L. P. Shi, R. Zhao, P. K. Tan, J. M. Li, H. K. Lee, X. S. Miao, A. Y. Du, and C. H. Tung, Phase change random access memory cell with superlattice-like structure, *Appl. Phys. Lett*., **88**(12):122114, 2006.
40. C. Xu, Z. Song, B. Liu, S. Feng, and B. Chen, Lower current operation of phase change memory cell with a thin TiO_2 layer, *Appl. Phys. Lett*., **92**(6):062103, 2008.
41. F. Rao, Z. Song, L. Wu, Y. Gong, S. Feng, and B. Chen, Phase change memory cell based on Sb2Te3/TiN/Ge2Sb2Te5 sandwich-structure, *Solid-State Electron*., **53**(3):276–278, 2009.
42. T. D. Happ, M. Breitwisch, A. Schrott, J. B. Philipp, M. H. Lee, R. Cheek, T. Nirschl, M. Lamorey, C. H. Ho, S. H. Chen, C. F. Chen, E. Joseph, S. Zaidi, G. W. Burr, B. Yee, Y. C. Chen, S. Raoux, H. L. Lung, R. Bergmann, and C. Lam, Novel one-mask self-heating pillar phase change memory, *Symposium on VLSI Technology, Digest of Technical Papers*, pp. 120–121, 2006.
43. S. L. Cho, J. H. Yi, Y. H. Ha, B. J. Kuh, C. M. Lee, J. H. Park, S. D. Nam, H. Horii, B. K. Cho, K. C. Ryoo, S. O. Park, H. S. Kim, U. I. Chung, J. T. Moon, and B. I. Ryu, Highly scalable on-axis confined cell structure for high density PRAM beyond 256Mb, *Symposium on VLSI Technology 2005, Digest of Technical Papers*, pp. 96–97, 2005.
44. H. Horii, J. H. Yi, J. H. Park, Y. H. Ha, I. G. Baek, S. O. Park, Y. N. Hwang, S. H. Lee, Y. T. Kim, K. H. Lee, U. I. Chung, and J. T. Moon, A novel cell technology using N-doped GeSbTe films for phase change RAM, *Symposium on VLSI Technology 2003, Digest of Technical Papers*, pp. 177–178, 2003.
45. F. Yeung, S.-J. Ahn, Y.-N. Hwang, C.-W. Jeong, Y.-J. Song, S.-Y. Lee, S.-H. Lee, K.-C. Ryoo, J.-H. Park, J.-M. Shin, W.-C. Jeong, Y.-T. Kim, G.-H. Koh, G.-T. Jeong, H.-S. Jeong, and K. Kim, Ge2Sb2Te5 Confined structures and integration of 64 Mb phase-change random access memory, *Jpn. J. Appl. Phys.*, **44**(4B):2691–2695, 2005.
46. Y. H. Ha, J. H. Yi, H. Horii, J. H. Park, S. H. Joo, S. O. Park, U. I. Chung, and J. T. Moon, An edge contact type cell for phase change RAM featuring very low power consumption, *Symposium on VLSI Technology 2003, Digest of Technical Papers*, pp. 175–176, 2003.
47. E. Small, S. M. Sadeghipour, L. Pileggi, and M. Asheghi, Thermal analyses of confined cell design for phase change random access memory (PCRAM), *11th Intersociety Conference on Thermal and Thermomechanical Phenomena in Electronic Systems*, pp. 1046–1054, 2008.
48. S. Hudgens and B. Johnson, Overview of phase-change chalcogenide nonvolatile memory technology, *MRS Bull*., **29**:829–832, 2004.

49. M. Wuttig, Phase-change materials: Towards a universal memory? *Nat. Mater.*, **4**(4):265–266, 2005.

50. M. H. R. Lankhorst, B. W. S. M. M. Ketelaars, and R. A. M. Wolters, Low-cost and nanoscale non-volatile memory concept for future silicon chips, *Nat. Mater.*, **4**(4):347–352, 2005.

51. M. Wuttig and N. Yamada, Phase-change materials for rewriteable data storage, *Nat. Mater.*, **6**(11):824–832, 2007.

52. A. L. Lacaita, D. Ielmini, and D. Mantegazza, Status and challenges of phase change memory modeling, *Solid-State Electron.*, **52**(9):1443–1451, 2008.

53. D. G. Cahill, W. K. Ford, K. E. Goodson, G. D. Mahan, A. Majumdar, H. J. Maris, R. Merlin, and S. R. Phillpot, Nanoscale thermal transport, *J. Appl. Phys.*, **93**(2):793–818, 2003.

54. D. G. Cahill, K. Goodson, and A. Majumdar, Thermometry and thermal transport in micro/nanoscale solid-state devices and structures, *J. Heat Transfer*, **124**(2):223–241, 2002.

55. E. T. Swartz and R. O. Pohl, Thermal boundary resistance, *Rev. Mod. Phys.*, **61**(3):605–668, 1989.

56. G. L. Pollack, Kapitza resistance, *Rev. Mod. Phys.*, **41**(1):48–81, 1969.

57. J. Feinleib, J. deNeufville, S. C. Moss, and S. R. Ovshinsky, Rapid reversible light-induced crystallization of amorphous semiconductors, *Appl. Phys. Lett.*, **18**(6):254–257, 1971.

58. E. J. Evans J. H. Helbers, and S. R. Ovshinsky, Reversible conductivity transformations in chalcogenide alloy films, *J. Non-Cryst. Solids*, **2**:334–346, 1970.

59. A. Bienenstock, F. Betts, and S. R. Ovshinsky, Structural studies of amorphous semiconductors, *J. Non-Cryst. Solids*, **2**:347–357, 1970.

60. S. Ovshinsky and H. Fritzsche, Reversible structural transformations in amorphous semiconductors for memory and logic, *Metall. Mater. Trans. B*, **2**(3):641–645, 1971.

61. H.-K. Lyeo, D. G. Cahill, B.-S. Lee, J. R. Abelson, M.-H. Kwon, K.-B. Kim, S. G. Bishop, and B.-K. Cheong, Thermal conductivity of phase-change material Ge2Sb2Te5, *Appl. Phys. Lett.*, **89**:151904, 2006.

62. M. H. Cohen, R. G. Neale, and A. Paskin, A model for an amorphous semiconductor memory device, *J. Non-Cryst. Solids*, **8-10**:885–891, 1972.

63. A. G. Steventon, The switching mechanisms in amorphous chalcogenide memory devices, *J. Non-Cryst. Solids*, **21**(3):319–329, 1976.

64. V. Weidenhof, I. Friedrich, S. Ziegler, and M. Wuttig, Laser induced crystallization of amorphous $Ge_2Sb_2Te_5$ films, *J. Appl. Phys.*, **89**(6):3168–3176, 2001.

65. P. K. Khulbe, E. M. Wright, and M. Mansuripur, Crystallization behavior of as-deposited, melt quenched, and primed amorphous states of $Ge_2Sb_{2.3}Te_5$ films, *J. Appl. Phys.*, **88**(7):3926–3933, 2000.

66. H.-Y. Cheng, S. Raoux, and Y.-C. Chen, The impact of film thickness and melt-quenched phase on the phase transition characteristics of $Ge_2Sb_2Te_5$, *J. Appl. Phys.*, **107**(7):074308, 2010.

67. S. Raoux, J. L. Jordan-Sweet, and A. J. Kellock, Crystallization properties of ultrathin phase change films, *J. Appl. Phys.*, **103**(11):114310, 2008.

68. H.-Y. Cheng, S. Raoux, and J. L. Jordan-Sweet, The crystallization behavior of stoichiometric and off-stoichiometric Ga–Sb–Te materials for phase-change memory, *Appl. Phys. Lett.*, **98**(12):121911, 2011.

69. N. Yamada, E. Ohno, K. Nishiuchi, N. Akahira, and M. Takao, Rapid-phase transitions of GeTe-Sb_2Te_3 pseudobinary amorphous thin films for an optical disk memory, *J. Appl. Phys.*, **69**(5):2849–2856, 1991.

70. D.-S. Suh, C. Kim, K. H. P. Kim, Y.-S. Kang, T.-Y. Lee, Y. Khang, T. S. Park, Y.-G. Yoon, J. Im, and J. Ihm, Thermoelectric heating of $Ge_2Sb_2Te_5$ in phase change memory devices, *Appl. Phys. Lett*., **96**(12):123115, 2010.

71. S. W. Ryu, H.-K. Lyeo, J. H. Lee, Y. B. Ahn, G. H. Kim, C. H. Kim, S. G. Kim, S.-H. Lee, K. Y. Kim, J. H. Kim, W. Kim, C. S. Hwang, and H. J. Kim, SiO_2 doped $Ge_2Sb_2Te_5$ thin films with high thermal efficiency for applications in phase change random access memory, *Nanotechnology*, **22**(25):254005, 2011.

72. J. Dresner, and G. B. Stringfellow, Electronic processes in the photo-crystallization of vitreous selenium, *J. Phys. Chem. Solids*, **29**(2):303–311, 1968.

73. M. Konishi, H. Santo, Y. Hongo, K. Tajima, M. Hosoi, and T. Saiki, Ultrafast amorphization in $Ge_{10}Sb_2Te_{13}$ thin film induced by single femtosecond laser pulse, *Appl. Opt*., **49**(18):3470–3473, 2010.

74. C. N. Afonso, J. Solis, F. Catalina, and C. Kalpouzos, Ultrafast reversible phase change in GeSb films for erasable optical storage, *Appl. Phys. Lett*., **60**(25):3123–3125, 1992.

75. S. D. Brorson, A. Kazeroonian, J. S. Moodera, D. W. Face, T. K. Cheng, E. P. Ippen, M. S. Dresselhaus, and G. Dresselhaus, Femtosecond room-temperature measurement of the electron-phonon coupling constant γ in metallic superconductors, *Phys. Rev. Lett.*, **64**(18):2172–2175, 1990.

76. A. V. Kolobov, A. S. Mishchenko, P. Fons, S. M. Yakubenya, and J. Tominaga, A possible mechanism of ultrafast amorphization in phase-change memory alloys: An ion slingshot from the crystalline to amorphous position, *J. Phys.: Cond. Matter*, **19**(45):455209, 2007.

77. J. L. F. Da Silva, A. Walsh, S.-H. Wei, and H. Lee, Atomistic origins of the phase transition mechanism in $Ge_2Sb_2Te_5$, *J. Appl. Phys.*, **106**(11):113509, 2009.

78. J. Lee, S. Kim, R. Jeyasingh, M. Asheghi, H. S. P. Wong, and K. E. Goodson, Microthermal stage for electrothermal characterization of phase-change memory, *IEEE Electron Device Lett*., **32**(7):952–954, 2011.

79. I. M. Khalatnikov and I. N. Adamenko, Theory of the Kapitza temperature discontinuity at a solid body-liquid helium boundary, *Sov. J. Exp. Theor. Phys*., **36**(3):391–394, 1973.

80. G. D. Mahan and M. Bartkowiak, Wiedemann-Franz law at boundaries, *Appl. Phys. Lett*., **74**(7):953–954, 1999.

81. A. Majumdar and P. Reddy, Role of electron-phonon coupling in thermal conductance of metal-nonmetal interfaces, *Appl. Phys. Lett*., **84**(23):4768–4770, 2004.

82. W. K. Njoroge, H.-W. Woltgens, and M. Wuttig, Density changes upon crystallization of $Ge_2Sb_{2.04}$ $Te_{4.74}$ films, *J. Vac. Sci. Technol. A*, **20**(1):230–233, 2002.

83. V. Giraud, J. Cluzel, V. Sousa, A. Jacquot, A. Dauscher, B. Lenoir, H. Scherrer, and S. Romer, Thermal characterization and analysis of phase change random access memory, *J. Appl. Phys.*, **98**:013520, 2005.

84. J. Lee, Z. Li, J. P. Reifenberg, S. Lee, R. Sinclair, M. Asheghi, and K. E. Goodson, Thermal conductivity anisotropy and grain structure in $Ge_2Sb_2Te_5$ films, *J. Appl. Phys.*, **109**:084902, 2011.

85. D. G. Cahill, S. K. Watson, and R. O. Pohl, Lower limit to the thermal conductivity of disor-

dered crystals, *Phys. Rev. B*, **46**(10):6131–6140, 1992.

86. T. Blachowicz, M. G. Beghi, G. Guntherodt, B. Beschoten, H. Dieker, and M. Wuttig, Crystalline phases in the $GeSb_2Te_4$ alloy system: Phase transitions and elastic properties, *J. Appl. Phys.*, **102**(9):093519, 2007.
87. M. Kuwahara, O. Suzuki, N. Taketoshi, Y. Yamakawa, T. Yagi, P. Fons, K. Tsutsumi, M. Suzuki, T. Fukaya, J. Tominaga, and T. Baba, Measurements of temperature dependence of optical and thermal properties of optical disk materials, *Jpn. J. Appl. Phys.*, **45**:1419–1421, 2006.
88. T. Vasilos and W. D. Kingery, Thermal conductivity: XI, Conductivity of some refractory carbides and nitrides, *J. Am. Ceram. Soc.*, **37**(9):409–414, 1954.
89. R. M. Costescu, M. A. Wall, and D. G. Cahill, Thermal conductance of epitaxial interfaces, *Phys. Rev. B*, **67**(5):054302, 2003.
90. T. Kato and K. Tanaka, Electronic properties of amorphous and crystalline $Ge_2Sb_2Te_5$, *Jpn. J. Appl. Phys.*, **44**(10):7340–7344, 2005.
91. F. Rao, Z. Song, L. Wu, B. Liu, S. Feng, and B. Chen, Investigation on the stabilization of the median resistance state for phase change memory cell with doublelayer chalcogenide films, *Appl. Phys. Lett.*, **91**(12):123511, 2007.
92. L. De Bellis, P. E. Phelan, and R. S. Prasher, Variations of acoustic and diffuse mismatch models in predicting thermal-boundary resistance, *J. Thermophys. Heat Transfer*, **14**(2):144–150, 2000.
93. R. Prasher, Acoustic mismatch model for thermal contact resistance of van der Waals contacts, *Appl. Phys. Lett.*, **94**(4):041905, 2009.
94. P. K. Schelling, S. R. Phillpot, and P. Keblinski, Phonon wave-packet dynamics at semiconductor interfaces by molecular-dynamics simulation, *Appl. Phys. Lett.*, **80**(14):2484–2486, 2002.
95. G. Fagas, A. G. Kozorezov, C. J. Lambert, J. K. Wigmore, A. Peacock, A. Poelaert, and R. den Hartog, Lattice dynamics of a disordered solid-solid interface, *Phys. Rev. B*, **60**(9):6459–6464 1999.
96. S. Pettersson and G. D. Mahan, Theory of the thermal boundary resistance between dissimilar lattices, *Phys. Rev. B*, **42**(12):7386–7390, 1990.
97. R. J. Stevens, L. V. Zhigilei, and P. M. Norris, Effects of temperature and disorder on thermal boundary conductance at solid-solid interfaces: Nonequilibrium molecular dynamics simulations, *Int. J. Heat Mass Transfer*, **50**(19-20):3977–3989, 2007.
98. R. J. Stevens, A. N. Smith, and P. M. Norris, Measurement of thermal boundary conductance of a series of metal-dielectric interfaces by the transient thermoreflectance technique, *J. Heat Transfer*, **127**(3):315–322, 2005.
99. M. L. Huberman and A. W. Overhauser, Electronic Kapitza conductance at a diamond-Pb interface, *Phys. Rev. B*, **50**(5):2865–2873, 1994.
100. B. C. Gundrum, D. G. Cahill, and R. S. Averback, Thermal conductance of metal-metal interfaces, *Phys. Rev. B*, **72**(24):245426, 2005.
101. W. A. Little, The transport of heat between dissimilar solids at low temperatures, *Can. J. Phys*., **37**(3):334–349, 1959.
102. A. V. Sergeev, Electronic Kapitza conductance due to inelastic electron-boundary scattering, *Phys. Rev. B*, **58**(16):R10199–R10202, 1998.

103. D. G. Cahill, Thermal conductivity measurement from 30 to 750K: The 3ω method, *Rev. Sci. Instrum*., **61**(2):802–808, 1990.

104. C. Peng and M. Mansuripur, Measurement of the thermal conductivity of erasable phase-change optical recording media, *Appl. Opt*., **39**(14):2347–2352, 2000.

105. E. R. Meinders and C. Peng, Melt-threshold method to determine the thermal conductivity of thin films in phase-change optical recording stacks, *J. Appl. Phys.*, **93**(6):3207–3213, 2003.

106. J. L. Battaglia, A. Kusiak, V. Schick, A. Cappella, C. Wiemer, M. Longo, and E. Varesi, Thermal characterization of the SiO_2-$Ge_2Sb_2Te_5$ interface from room temperature up to 400°C, *J. Appl. Phys.*, **107**(4):044314, 2010.

107. J. Lee, J. P. Reifenberg, E. Bozorg-Grayeli, L. Hom, L. Zijian, K. SangBum, M. Asheghi, H. S. P. Wong, and K. E. Goodson, Decoupled thermal resistances of phase change material and their impact on PCM devices, *12th IEEE Intersociety Conference on Thermal and Thermomechanical Phenomena in Electronic Systems (ITherm)*, pp. 1–6, 2010.

108. S. M. Lee and D. G. Cahill, Heat transport in thin dielectric films, *J. Appl. Phys.*, **81**(6):2590–2595, 1997.

109. W. P. Risk, C. T. Rettner, and S. Raoux, In situ 3 omega techniques for measuring thermal conductivity of phase-change materials, *Rev. Sci. Instrum*., **79**(2):026108, 2008.

110. W. P. Risk, C. T. Rettner, and S. Raoux, Thermal conductivities and phase transition temperatures of various phase-change materials measured by the 3 omega method, *Appl. Phys. Lett*., **94**(10):101906, 2009.

111. R. Fallica, J.-L. Battaglia, S. Cocco, C. Monguzzi, A. Teren, C. Wiemer, E. Varesi, R. Cecchini, A. Gotti, and M. Fanciulli, Thermal and electrical characterization of materials for phase-change memory cells, *J. Chem. Eng. Data*, **54**(6):1698–1701, 2009.

112. B. W. Olson, S. Graham, and K. Chen, A practical extension of the 3 omega method to multilayer structures. *Rev. Sci. Instrum*., **76**(5):053901, 2005.

113. C. Dames and G. Chen, 1 omega, 2 omega, and 3 omega methods for measurements of thermal properties, *Rev. Sci. Instrum*., **76**(12):124902, 2005.

114. T. Borca-Tasciuc, A. R. Kumar, and G. Chen, Data reduction in 3 omega method for thin-film thermal conductivity determination, *Rev. Sci. Instrum*., **72**(4):2139–2147, 2001.

115. J. Kimling, S. Martens, and K. Nielsch, Thermal conductivity measurements using 1 omega and 3 omega methods revisited for voltage-driven setups, *Rev. Sci. Instrum*., **82**(7):074903, 2011.

116. M. Kuwahara, O. Suzuki, N. Taketoshi, T. Yagi, P. Fons, J. Tominaga, and T. Baba, Thermal conductivity measurements of Sb-Te alloy thin films using a nanosecond thermoreflectance measurement system, *Jpn. J. Appl. Phys.*, **46**(10A):6863–6864, 2007.

117. M. Kuwahara, O. Suzuki, Y. Yamakawa, N. Taketoshi, T. Yagi, P. Fons, T. Fukaya, J. Tominaga, and T. Baba, Temperature dependence of the thermal properties of optical memory materials, *Jpn. J. Appl. Phys.*, **46**:3909–3911, 2007.

118. L. E. Shelimova, O. G. Karpinskii, P. P. Konstantinov, M. A. Kretova, E. S. Avilov, and V. S. Zemskov, Composition and properties of layered compounds in the GeTe–Sb2Te3 system, *Inorg. Mater*., **37**(4):342–348, 2001.

119. Y. Yang, C. T. Li, S. M. Sadeghipour, H. Dieker, M. Wuttig, and M. Asheghi, Thermal characterization of dielectric and phase change materials for the optical recording applications, *J. Appl. Phys.*, **100**(2):024102, 2006.

120. E. Bozorg-Grayeli, J. P. Reifenberg, K. W. Chang, M. Panzer, and K. E. Goodson, Thermal conductivity and boundary resistance measurements of GeSbTe and electrode materials using nanosecond thermoreflectance, *12th IEEE Intersociety Conference on Thermal and Thermomechanical Phenomena in Electronic Systems (ITherm)*, pp. 1–7, 2010.

121. J. Lee, Z. Li, J. P. Reifenberg, S. Lee, R. Sinclair, M. Asheghi, and K. E. Goodson, Thermal conductivity anisotropy and grain structure in $Ge_2Sb_2Te_5$ films, *J. Appl. Phys.*, **109**(8):084902, 2011.

122. Z. Li, J. Lee, J. P. Reifenberg, M. Asheghi, R. G. D. Jeyasingh, H. P. Wong, and K. E. Goodson, Grain boundaries, phase impurities, and anisotropic thermal conduction in phase-change memory, *IEEE Electron Device Lett.*, **32**(7):961–963, 2011.

123. Y. S. Ju and K. E. Goodson, Process-dependent thermal transport properties of silicon-dioxide films deposited using low-pressure chemical vapor deposition, *J. Appl. Phys.*, **85**(10):7130–7134, 1999.

124. C. Peng and M. Mansuripur, Measurement of the thermal coefficients of rewritable phase-change optical recording media, *Appl. Opt.*, **41**(2):361–369, 2002.

125. K. E. Goodson, O. W. Käding, M. Rösler, and R. Zachai, Experimental investigation of thermal conduction normal to diamond-silicon boundaries, *J. Appl. Phys.*, **77**:1385–1392, 1995.

126. M. A. Panzer, G. Zhang, D. Mann, X. Hu, E. Pop, H. Dai, and K. E. Goodson, Thermal properties of metal-coated vertically aligned single-wall nanotube arrays, *J. Heat Transfer*, **130**(5):052401, 2008.

127. W. J. Parker, R. J. Jenkins, C. P. Butler, and G. L. Abbott, Flash method of determining thermal diffusivity, heat capacity, and thermal conductivity, *J. Appl. Phys.*, **32**(9):1679–1684, 1961.

128. T. Q. Qiu, C. P. Grigoropoulos, and C. L. Tien, Novel technique for noncontact and microscale temperature measurements, *Exp. Heat Transfer*, **6**(3):231–241, 1993.

129. C. A. Paddock and G. L. Eesley, Transient thermoreflectance from thin metal films, *J. Appl. Phys.*, **60**(1):285–290, 1986.

130. D. G. Cahill, Analysis of heat flow in layered structures for time-domain thermoreflectance, *Rev. Sci. Instrum.*, **75**(12):5119–5122, 2004.

131. A. Schmidt, M. Chiesa, X. Chen, and G. Chen, An optical pump-probe technique for measuring the thermal conductivity of liquids, *Rev. Sci. Instrum.*, **79**(6):064902, 2008.

132. M. A. Panzer, M. Shandalov, J. A. Rowlette, Y. Oshima, C. Yi Wei, P. C. McIntyre, and K. E. Goodson, Thermal properties of ultrathin hafnium oxide gate dielectric films, *IEEE Electron Device Lett.*, **30**(12):1269–1271, 2009.

133. W. S. Capinski and H. J. Maris, Improved apparatus for picosecond pump-and-probe optical measurements, *Rev. Sci. Instrum.*, **67**(6):2720–2726, 1996.

134. P. M. Norris, A. P. Caffrey, R. J. Stevens, J. M. Klopf, J. J. T. McLeskey, and A. N. Smith, Femtosecond pump–probe nondestructive examination of materials (Invited), *Rev. Sci. Instrum.*, **74**(1):400–406, 2003.

135. J. Lee, J. P. Reifenberg, L. Zijian, L. Hom, M. Asheghi, K. SangBum, H. S. P. Wong, and K. E. Goodson, Measurement of anisotropy in the thermal conductivity of $Ge_2Sb_2Te_5$ films, *10th Annual Non-Volatile Memory Technology Symposium*, 2009.

136. J. P. Reifenberg, D. L. Kencke, and K. E. Goodson, The impact of thermal boundary resistance in phase-change memory devices, *IEEE Electron Device Lett.*, **29**(10):1112–1114,

2008.

137. B.-S. Lee, J. R. Abelson, S. G. Bishop, D.-H. Kang, B.-k. Cheong, and K.-B. Kim, Investigation of the optical and electronic properties of $Ge_2Sb_2Te_5$ phase change material in its amorphous, cubic, and hexagonal phases, *J. Appl. Phys*., **97**(9):093509, 2005.

138. L. Shelimova, O. Karpinskii, V. Zemskov, and P. Konstantinov, Structural and electrical properties of layered tetradymite-like compounds in the GeTe-Bi_2Te_3 and GeTe-Sb_2Te_3 systems, *Inorg. Mater*., **36**(3):235–242, 2000.

139. N. G. Ptitsina, G. M. Chulkova, K. S. Il'in, A. V. Sergeev, F. S. Pochinkov, E. M. Gershenzon, and M. E. Gershenson, Electron-phonon interaction in disordered metal films: The resistivity and electron dephasing rate, *Phys. Rev. B*, **56**(16):10089–10096, 1997.

140. J. Lee, S. Kim, A. Marconnet, M. A. A. in 't Zandt, M. Asheghi, H.-S. P. Wong, and K. E. Goodson, Thermoelectric characterization and power generation using a silicon-on-insulator substrate, *J. Microelectromech. Syst*., **21**:2175704, 2011.

141. M. N. Schneider, T. Rosenthal, C. Stiewe, and O. Oeckler, From phase-change materials to thermoelectrics? *Zeit. Kristall*., **225**:463–470, 2010.

142. H. Ohta, S. Kim, Y. Mune, T. Mizoguchi, K. Nomura, S. Ohta, T. Nomura, Y. Nakanishi, Y. Ikuhara, M. Hirano, H. Hosono, and K. Koumoto, Giant thermoelectric Seebeck coefficient of a two-dimensional electron gas in SrTiO3, *Nat. Mater.*, **6**(2):129–134, 2007.

143. J. Y. Sungtaek, and U. Ghoshal, Study of interface effects in thermoelectric microrefrigerators, *J. Appl. Phys*., **88**(7):4135–4139, 2000.

144. Y. Jung, R. Agarwal, C.-Y. Yang, and R. Agarwal, Chalcogenide phase-change memory nanotubes for lower writing current operation, *Nanotechnology*, **22**(25):254012, 2011.

145. J. Chen, T. Sun, D. Sim, H. Peng, H. Wang, S. Fan, H. H. Hng, J. Ma, F. Y. C. Boey, S. Li, M. K. Samani, G. C. K. Chen, X. Chen, T. Wu, and Q. Yan, Sb_2Te_3 nanoparticles with enhanced Seebeck coefficient and low thermal conductivity, *Chem. Mater*., **22**(10):3086–3092, 2010.

146. T.-Y. Lee, K. H. P. Kim, D.-S. Suh, C. Kim, Y.-S. Kang, D. G. Cahill, D. Lee, M.-H. Lee, M.-H. Kwon, K.-B. Kim, and Y. Khang, Low thermal conductivity in $Ge_2Sb_2Te_5$–SiO_x for phase change memory devices. *Appl. Phys. Lett*., **94**(24):243103, 2009.